Chapter 2

Optical Performance Predictions for Asymmetric Compound Parabolic Photovoltaic Concentrators: A Ray Trace Analysis

2.1 Introduction

Ray tracing (Welford and Winston, 1989, Glassner, 1991) can be used to determine the optical performance of solar energy systems. Ray trace techniques have been used to model the energy distribution of solar energy collectors with tubular, inverted absorber for solar thermal applications (Eames and Norton, 1993a, Eames et al., 2001) and asymmetric CPC for photovoltaic applications (Zaropoulos et al., 2000, Mallick et al., 2001, 2002a). It is assumed that all rays of interest are specular i.e. the angle of incidence equals the angle of reflection The incident direct solar flux at the aperture is assumed to be a number of parallel rays each carrying equal amounts of energy. Vector forms of reflection and refraction laws are applied to the ray trace in the solar energy system (Welford, 1978). From the law of reflection

$$\vec{r}_{refl} = \vec{r}_{inc} - 2\left(\mathbf{n} \bullet \vec{r}_{inc}\right)\ \mathbf{n} \qquad (2.1.1)$$

and from the law of refraction

$$n_r \vec{r}_{refr} = n_i \vec{r}_{inc} + \left(n_r \vec{r}_{refr} \bullet \mathbf{n} - n_i \vec{r}_{inc} \bullet \mathbf{n}\right)\ \mathbf{n} \qquad (2.1.2)$$

and incident ray, reflected ray and the normal to the surface are all in the same plane. This can be represented in mathematical terms as:

i. no phase space change between the scalar product of the incident ray and the reflected ray
ii. the vector product of the incident and reflected ray with the dot product of the normal vector becomes zero.

Rays entering a concentrating collector intersect with the aperture cover and then as shown in figure 2.1.1, either (Eames, 1990)

i. strike the absorber (PV) with no previous reflections
ii. reflect a finite number of times before intersecting with the absorber
iii. reflect a finite number of times before exiting from the collector reflected back out through the aperture.

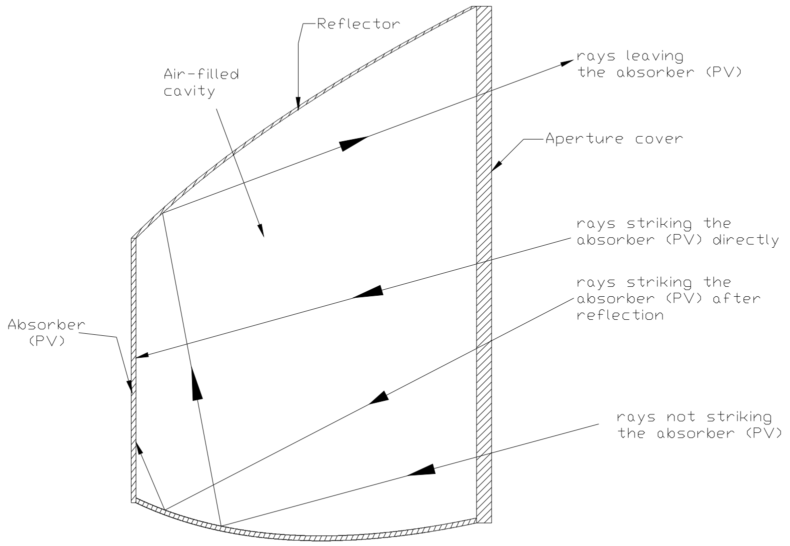

Figure 2.1.1 A ray which enters an ACPC collector with a flat absorber (PV) either: (i) strikes the absorber (PV) with no reflections, (ii) strikes the absorber (PV) after a number of reflections (iii) leaves the collector without reaching the absorber (PV) after a number of reflections.

In this chapter a two-dimensional ray trace technique is applied to line-axis asymmetric compound parabolic photovoltaic concentrators. The ray trace technique is applied to calculate the energy distributions at the aperture cover, reflector and the PV absorber. The calculated energy distributions provide the boundary conditions for the heat transfer model. Ray tracing is also used to determine the optical efficiency for selected asymmetric compound parabolic photovoltaic concentrators.

2.2 Generalised Two-Dimensional Ray Trace Technique for Line Axis Photovoltaic Concentrators

2.2.1 Rays Intersection at the Aperture Cover

A ray which is incident at the glass surface may be;

i. reflected back from the aperture surface
ii. absorbed by the aperture cover
iii. transmitted through the aperture cover.

Figure 2.2.1.1 illustrates these possibilities for rays incident on a glass aperture cover.

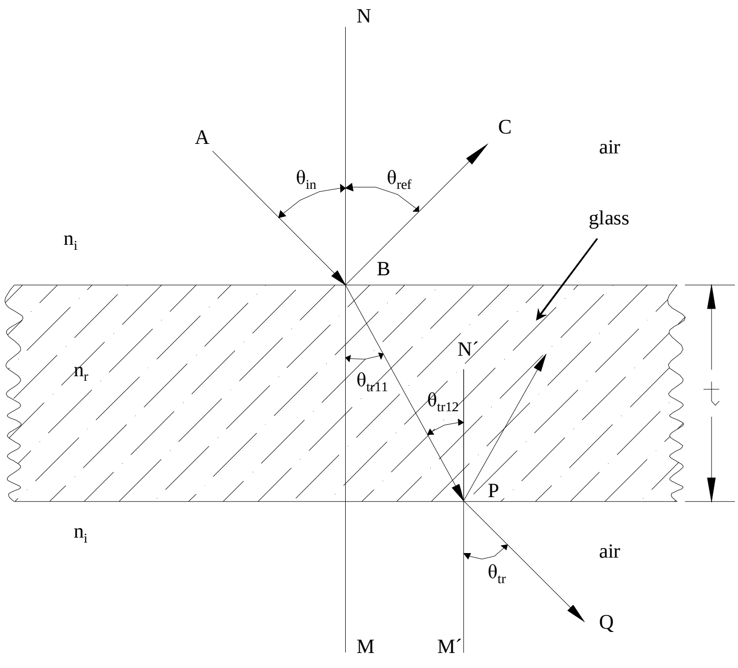

Figure 2.2.1.1 A solar ray incident on the glass aperture carries energy E_{in}. A part of the ray is reflected back from the glass surface, a part is absorbed and the rest is reflected from the outer surface.

The direction of the incoming and the outgoing rays after intersection with the aperture cover can be calculated using Snell's law (Norton, 1992)

$$\frac{\sin(\theta_{tr})}{\sin(\theta_{tr12})} = \frac{\sin(\theta_{in})}{\sin(\theta_{tr11})} \equiv \frac{n_r}{n_i} \qquad (2.2.1.1)$$

The ray incident at the aperture cover glass carries energy E_{in}, the reflected component can be calculate using the following equation (Duffie and Beckman, 1991)

$$E_{\nu} = \nu E_{in} \tag{2.2.1.2}$$

where for unpolarized radiation the reflective coefficient can be expressed as

$$\nu_{\perp} = \frac{\sin^2(\theta_{tr11} - \theta_{in})}{\sin^2(\theta_{tr11} + \theta_{in})} \tag{2.2.1.3}$$

$$\nu_{\mathrm{II}} = \frac{\tan^2(\theta_{tr11} - \theta_{in})}{\tan^2(\theta_{tr11} + \theta_{in})} \tag{2.2.1.4}$$

and

$$\nu = \frac{1}{2}(\nu_{\perp} + \nu_{\mathrm{II}}) \tag{2.2.1.5}$$

For normal incidence the reflective coefficient becomes

$$\nu_0 = \left(\frac{n_i - n_r}{n_i + n_r}\right)^2 \tag{2.2.1.6}$$

Internal absorption in a glass aperture can be calculated from the path length of the ray through the aperture cover. For an extinction coefficient ‘α’ and thickness ‘t’ of the aperture glass, the energy absorbed by the aperture cover becomes (Norton, 1992)

$$E_{\alpha} = E_{in} e^{-\alpha t} \tag{2.2.1.7}$$

In solar energy applications, transmission of radiation through a transparent glass cover can be considered as two films of same material that causes internal reflection loss. At off-normal incidence the radiation reflected at an interface is different for each component of polarization and therefore transmitted and reflected radiation become partially polarized. Taking this into account the transmittance for perpendicular and parallel component of polarization are (Norton, 1992)

$$\tau_{\perp} = \frac{1-\nu_{\perp}}{1+\nu_{\perp}} \tag{2.2.1.8}$$

and

$$\tau_{II} = \frac{1-\nu_{II}}{1+\nu_{II}} \tag{2.2.1.9}$$

therefore the transmittance becomes

$$\tau_r = \frac{1}{2}\left(\frac{1-\nu_{\perp}}{1+\nu_{\perp}} + \frac{1-\nu_{II}}{1+\nu_{II}}\right) \tag{2.2.1.10}$$

This transmitted energy can be written as

$$E_{tr} = \tau(E_{in}) \tag{2.2.1.11}$$

A closer approximation can be determined using the wavelength dependent transmittance. If there is no significant angular dependence of monochromatic transmittance, the transmittance for incident radiation of a spectral distribution is calculated by (Duffie and Beckman, 1991)

$$\tau = \sum_{i=1}^{n} \tau_{\lambda i} \Delta f_i \tag{2.2.1.12}$$

For an angular dependence of transmittance within the total angle θ equation (2.2.1.10) can be written as

$$\tau(\theta) = \frac{\int_0^\infty \tau_\lambda(\theta) I_{\lambda i}(\theta) d\lambda}{\int_0^\infty I_{\lambda i}(\theta) d\lambda} \tag{2.2.1.13}$$

2.2.2 **Rays Intersecting with the Reflector**

For a ray intersecting with the reflector a part of the energy carried by the ray is reflected back and the rest is absorbed by the reflector as shown in figure 2.2.2.1. The absorbed energy increases the reflector temperature and is diffused through the reflector by conduction. The energy absorbed by the reflector varies depending on the absorptance of the reflector. The ray trace model assumes that all rays are specular (Eames and Norton, 1993a)

$$\theta_{in} = \theta_{ref} \tag{2.2.2.1}$$

The energy absorbed by the reflector is determined by

$$E_\rho = (1-\rho) E_{tr} \tag{2.2.2.2}$$

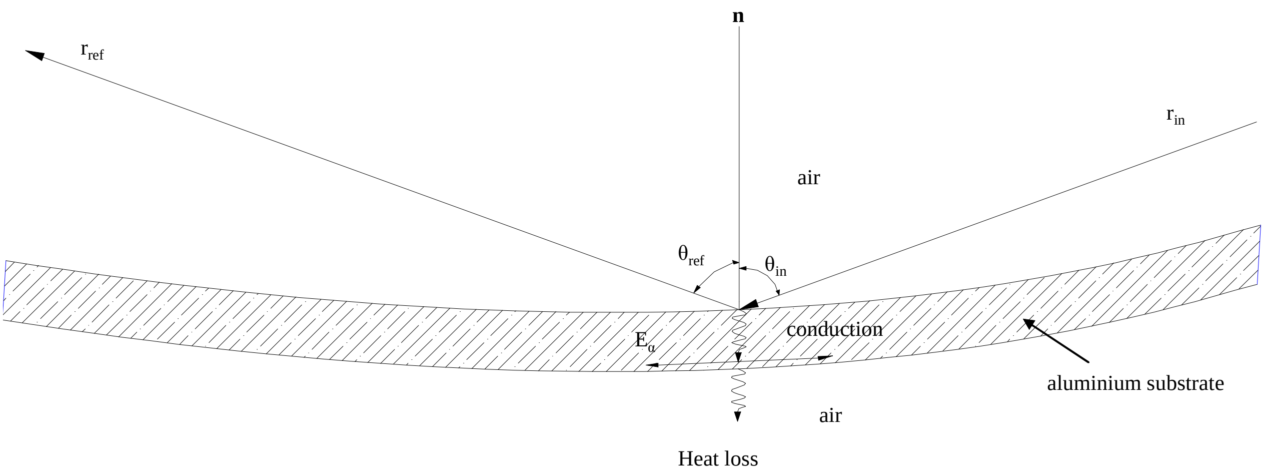

Figure 2.2.2.1 Rays intersect at the reflector, (i) a part is absorbed and (ii) the rest is reflected, onto the absorber (PV) or re-emitted at the aperture.

2.2.3 Rays Intersecting with the PV Absorber

In a line axis photovoltaic concentrator PV solar cells form the absorber, it is assumed that the PV cells are a perfect black body. Therefore, all incident energy will be absorbed by the photovoltaic solar cell and either converted in to electrical or thermal energy.

2.3 Influence of Angular Skyward Solar Radiation Distribution

Direct solar radiation can be modified by scattering processes. The major possibilities for solar rays before intersecting with an absorber (PV) surface (Duffie and Beckman, 1991) are that rays can either

- directly intersect with the collector surface without any change in their atmospheric path length
- be scattered diffusely by micro particles in the atmosphere like cloud, dust etc
- be directly incident onto the ground and reflected onto the absorber (PV) or back into the atmosphere and after reflection by atmospheric particles reach the absorber (PV).

In a comprehensive optical trace analysis it is important to simulate both direct and diffuse insolation components. To accomplish this, the aperture cover, reflector and PV absorber are divided into strips of equal width. The energy incident on the aperture is divided into the number of strips which followed by multiplication by its width gives the energy carried by each strip. It is assumed, the solar rays pass through the centre of each strip, when the number of strips tends to infinity this represents the actual insolation input.

To model the diffuse solar radiation incident on line axis photovoltaic concentrators, the three alternative angular skywards diffuse distributions given in equation 2.3.1 were considered (Prapas et al., 1987a);

$$\left.\begin{array}{ll} \textit{Isotropic}: & I_{D,\phi} = 1 \\ \textit{Cosine}: & I_{D,\phi} = \dfrac{\pi}{2}\cos\phi \\ \textit{Hybrid Gaussian}: & I_{D,\phi} = \rho_0 + k_{norm}(1-\rho_0)\dfrac{\pi}{\sigma\sqrt{2\pi}}e^{\left(-\frac{\phi^2}{2\sigma^2}\right)} \end{array}\right\} \tag{2.3.1}$$

These distributions are shown in figure 2.3.1. For solar incidence angles between –90º to +90º (i.e. 0º to 180º) at 2º intervals, 100,000 rays spaced equally were traced over the aperture surface. The energy flux incident at each component of the system is then calculated by the sum of energy absorbed from each and every individual ray incident at that component.

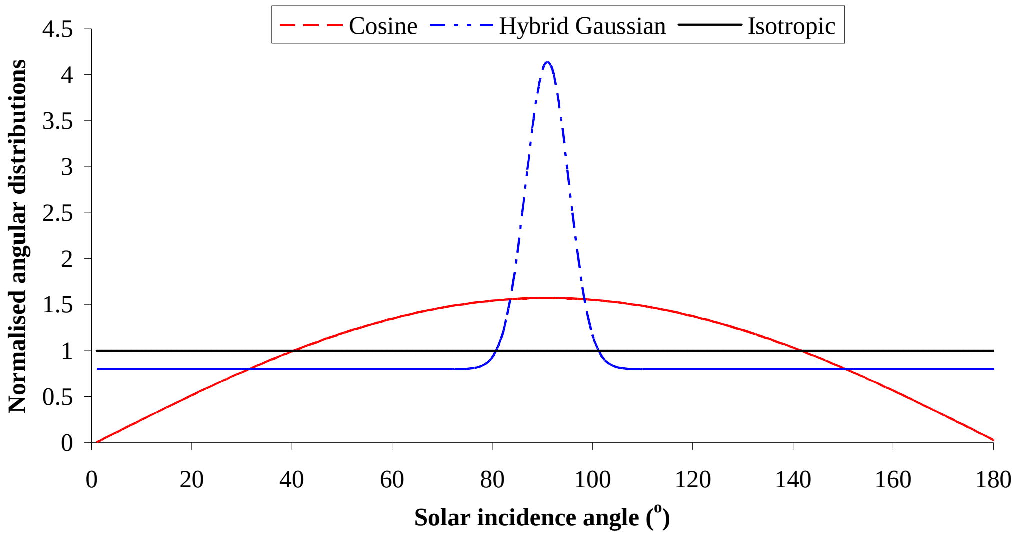

Figure 2.3.1 Three alternative skyward angular distributions of diffuse solar radiation (Prapas et al., 1987a).

2.4 Ray Trace Analysis Assumptions

The following assumptions were made for the ray trace analysis:

- All rays were specular i.e. whenever any reflection occurs, the incident ray, the reflected ray and the normal at the point of intersection are in same plane (i.e. $(\vec{r}_{inc} \times \vec{r}_{ref}) \bullet \mathbf{n} = 0$).
- All rays follow Fermat's principle i.e. a ray travels from one point (point A) to another point (point B) in the minimum distance and time (Lipson and Lipson, 1981). If a ray travels from a source point A to the intersecting point B this can be written $\int_A^B L(x,y)dt = 0$, where the path length L(x,y) between points A and B is a function of their co-ordinates.
- The second order statistics of the shape factor is neglected. Most rays have single or double reflection before they reach the absorber. As a result the gradient change between intermediate reflections is negligible.

2.5 Definition of Incidence Angle for the Ray Trace Analysis

Angles of incidence are measured in a clockwise direction from the vertical as shown in figure 2.5.1. For direct solar radiation, solar rays can be incident within the angular range of 0º to 180º.

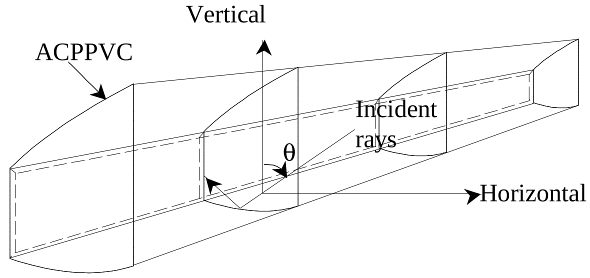

Figure 2.5.1 Incident angle definition used for the ACPPVC. The incidence angle is measured in a clock-wise direction from the vertical.

2.6 Ray Trace Analysis for Selected Asymmetric Compound Parabolic Photovoltaic Concentrators

Equation (2.3.1) was incorporated into the ray trace analysis program to determine the effects of the diffuse solar radiation incident on the system. The data generated included the energy distributions at the aperture, reflector and the absorber along with the co-ordinates of each of the rays incident on the aperture cover. Using a graphic software tool (Anon, 2001a) ray trace diagrams could be drawn for any incidence angle and solar radiation distribution. Detailed optical analysis was undertaken considering 100,000 rays incident on the glass aperture between angles 0° to 180° at 2° intervals. For illustration, ray traces for 50 incident rays are presented.

2.6.1 Comparative Ray Trace Diagram for an ACPPVC-50 and an ACPPVC-60

A ray trace analysis has been performed for both 50° and 60° effective acceptance-half angle asymmetric compound parabolic concentrators. The geometrical characteristics of two systems considered in the ray trace analysis are shown in table 2.6.1.

System geometry	System 1 (ACPPVC-50)		System 2 (ACPPVC-60)	
	Full CPC	Truncated CPC	Full CPC	Truncated CPC
Acceptance-half angles	50° & 0°	-	0° & 60°	-
Absorber width (mm)	50.0	50.0	50.0	50.0
Aperture width (mm)	116	100.4	100.0	87.0
Length of Reflector 1 (mm)	84.4	84.4	62.2	62.2
Length of Reflector 2 (mm)	202.8	93.3	157.8	73.8
Concentration ratio	2.32	2.01	2.0	1.74
Truncation (%) R1, R2	-	0, 54	-	0, 53

Table 2.6.1 Geometrical characteristics employed for the ray trace analysis.

Both photovoltaic concentrators have one acceptance-half angle of 0° and the same PV absorber widths but both concentrators have different aperture widths and thus different concentration ratios. The ray trace diagrams for the ACPPVC-50 and ACPPVC-60 are shown in figure 2.6.1.1. Figure 2.6.1.1(a) and figure 2.6.1.1(b) shows the ray trace diagram for an untruncated and truncated version of the ACPPVC-50 when the incident rays are at an angle of 60° to the glass aperture cover. It can be seen from the ray trace diagram that all rays incident at the glass aperture are either directly incident at the PV or absorbed by the PV after a finite number of reflections at the reflector. It can be seen from figure 2.6.1.1 that the number of reflections at the lower reflector is higher for the ACPPVC-50 compared to the ACPPVC-60 although the solar incidence angle at the aperture is 60° for both concentrators. This is because the concentration ratio of ACPPVC-50 is higher than that of the ACPPVC-60. This signifies the angular acceptance range for both concentrators is different, this is discussed further in section 2.7.1.

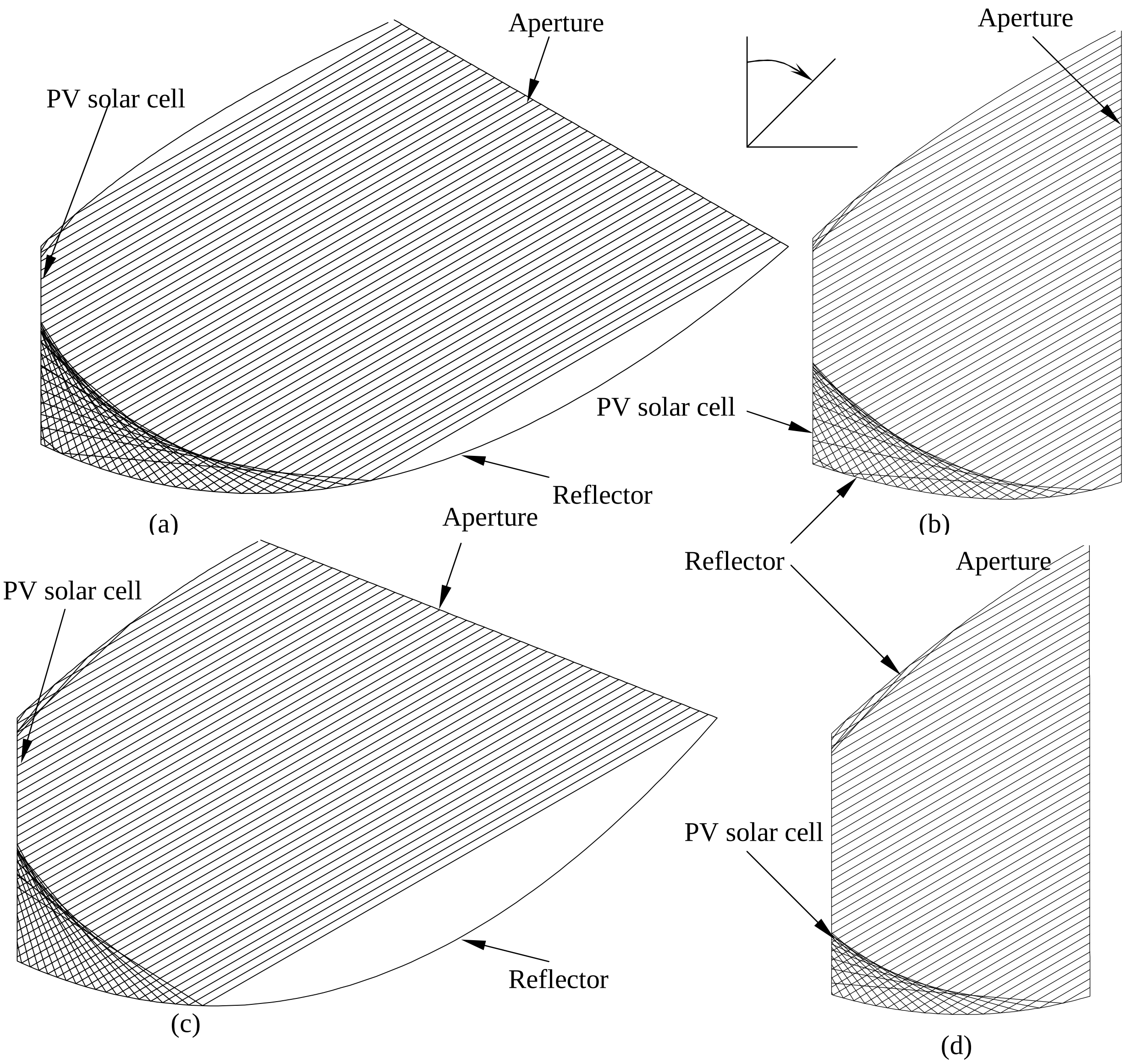

Figure 2.6.1.1 Ray trace diagrams for (a) untruncated ACPPVC-50, (b) truncated ACPPVC-50, (c) untruncated ACPPVC-60 and (d) truncated ACPPVC-60. No of incoming rays were 50 and the solar radiation intensity incident at an angle of 60°.

2.6.2 Ray Trace Diagram for the Untruncated Systems

Ray trace diagrams for the 50° effective acceptance-half angle untruncated ACPPVC for a range of solar incidence angles are shown in figure 2.6.2.1. The PV concentrator has a concentration ratio of 2.32 with 50 illustrative rays presented. Each ray carries an equal amount of energy, determined by dividing the number of rays incident on the aperture by the total incident insolation. It can be seen from figure 2.6.2.1(a) that when the solar incidence angle is less than 45° (to the vertical), some rays are reflected back out of the system. As direct solar incidence angle increases, the number of rays reflected at the lower reflector becomes less than the number of rays reflected at the upper reflector. It can be seen from figure 2.6.2.1(b) and figure 2.6.2.1(c) that although the number of rays reflected on both reflectors are not same for solar incidence angles of 60° and 75° all rays reach the PV surface. When the solar incidence angle is 90° i.e. solar rays are incident perpendicular to the vertical, rays miss the absorber surface and are reflected back out of the system. Based on this ray trace analysis the angular acceptance range can be predicted, this is discussed further in section 2.7.1

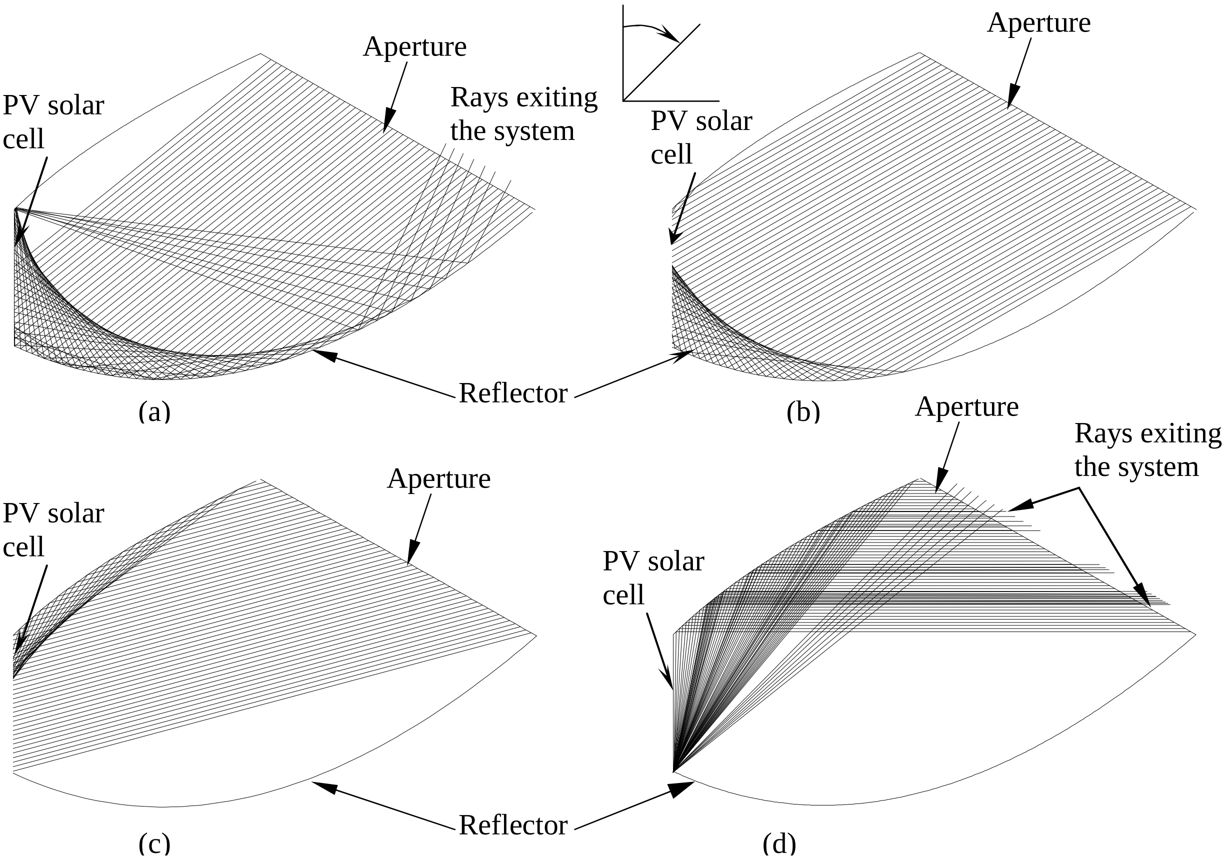

Figure 2.6.2.1 Ray trace diagram for untruncated ACPPVC-50 system for solar incidence angles of (a) 45° (b) 60° (c) 75° and (d) 89.5° (to the vertical) on the glass aperture cover. 50 rays are included for each ray trace diagram.

2.6.3 Ray Trace Diagram for a Truncated ACPPVC-50 System

Ray trace diagrams for a truncated ACPPVC-50 with solar incidence angles of 42°,60°, 75° and 89.5° from the vertical are shown in figure 2.6.3.1. Truncation provides a vertical aperture to facilitate integration in a plane building façade, each reflector is truncated by different amounts. Truncation reduces the quantity of reflector material and thus weight and cost. Figure 2.6.3.1 shows that 54% truncation of the ACPPVC-50 reduces the concentration ratio by 12%. It also can be seen from figures 2.6.3.1 (a) to 2.6.3.1 (d) that the number of reflections at the lower reflector increases as the solar incidence angle is increased. For solar incidence angles below 42º or above 90º, some of the solar rays are reflected back out of the system and miss the PV. This reduces the angular acceptance range for this system. However for any intermediate solar incidence angle (i.e. above 42º but below 90º) all rays reach the absorber although the number of reflections at both reflectors vary with incidence angle.

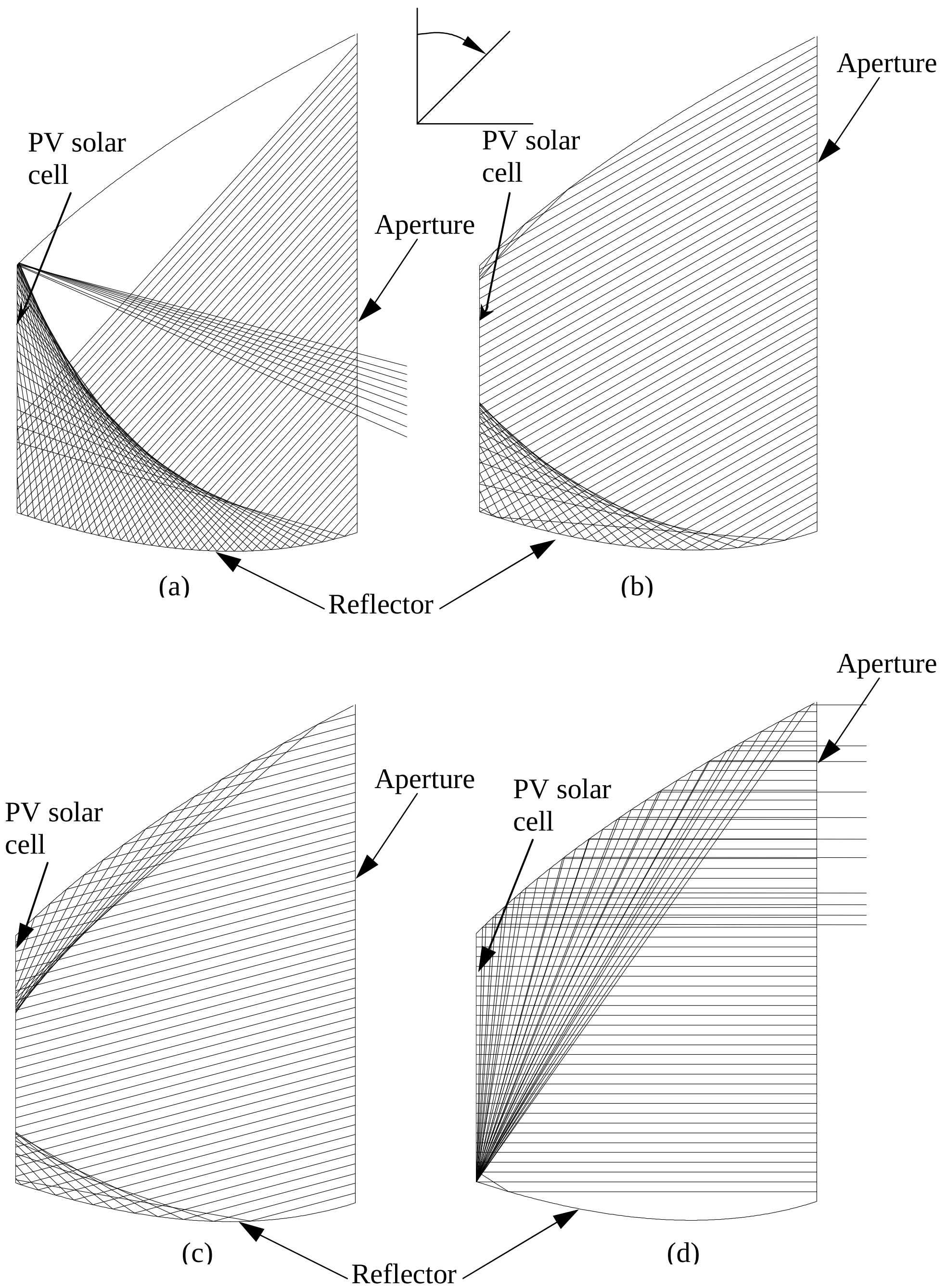

Figure 2.6.3.1 Examples of ray trace diagram for truncated ACPPVC-50 for solar incidence angles on the aperture cover glass of (a) 42°, (b) 60°, (c) 75° and (d) 89.5° to the vertical. 50 rays are included for each ray trace diagram.

2.6.4 **Ray Trace Diagrams for Systems Using Different Numbers of Planar Elements to Form the Reflector Profile**

Varying the number of planar elements that comprise the reflector surfaces allows the effects of cost-reducing simplifications in reflector geometry to be seen. Ray trace diagrams for an ACPPVC-50 in which the reflectors are approximated by three and five planar mirror sections along with their truncated counterparts are shown in figure 2.6.4.1. For each illustrative ray trace diagram the solar incidence angle was 60° to the vertical. It can be seen from the figure 2.6.4.1 (a) that of 50 incoming rays shown incident at the aperture only a single ray does not reach the absorber, for the truncated version of this system all rays shown reached the absorber. For both the three and five planar element system, truncation allows an increase in the angular acceptance range to achieve a collection efficiency of 100%. The ray trace diagrams for truncated three and five planar reflector elements of ACPPVC-50 are shown in figures 2.6.4.1 (c) and 2.6.4.1 (d) respectively.

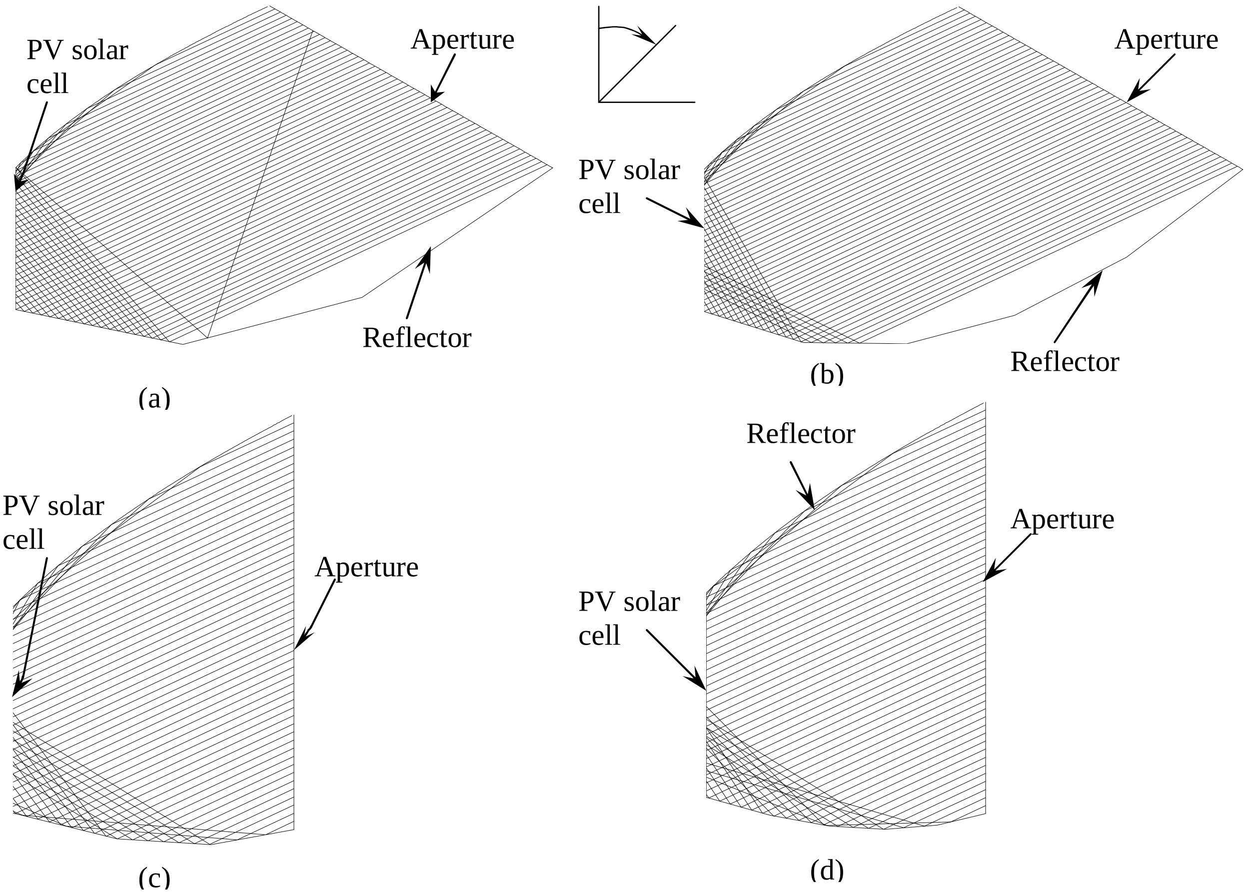

Figure 2.6.4.1 Ray trace diagrams for an ACPPVC-50 with the reflector profile approximated by different numbers of planar reflector elements (a) 3 elements, (b) 5 element, (c) truncated 3 element, and (d) truncated 5 element system. For each illustrative ray trace diagram the solar incidence angle was 60° to the vertical.

2.6.5 **Ray Trace Diagram for an ACPPVC-50 with Different PV Inclination Angles**

The asymmetric compound parabolic photovoltaic concentrator can be mounted at any inclination. The results of simulations undertaken for the ACPPVC-50 inclined at 0°, 5° and 10° to the vertical are presented in figure 2.6.5.1. In all ray trace diagrams, 50 rays are presented for a solar incidence angle of 44° to the vertical. From figure 2.6.5.1 it can be seen that the average number of reflections the rays undergo before reaching the PV decreases for the inclined systems. It can be seen from figure 2.6.5.1 (d) that the upper reflector is truncated by an identical amount to the previous vertically oriented system whereas the lower reflector has been truncated by an additional 8%.

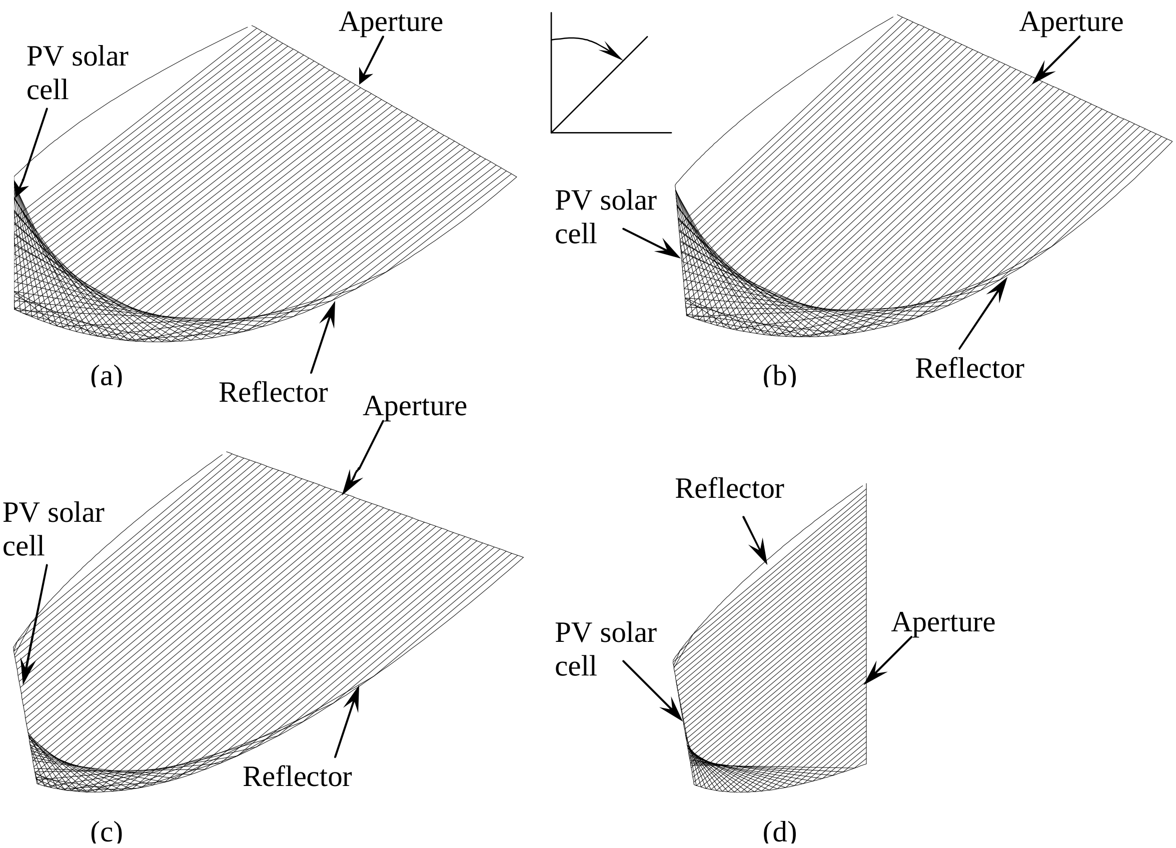

Figure 2.6.5.1 Ray trace diagrams for (a) 0° (b) 5°, (c) 10° inclined untruncated ACPPVC-50 and (d) a 10° inclined truncated ACPPVC-50. 50 rays are included for each ray trace diagram.

2.7 The Comparative Optical Performance of the Two Modelled Photovoltaic Concentrators

The optical performance of untruncated, truncated and inclined ACPPVC-50 and untruncated ACPPVC-60 were determined for a range of solar incidence angles. 100,000 rays equally spaced across the aperture cover were traced for all solar incidence angles from 0º to 180º at 1º intervals.

2.7.1 Angular Acceptance Functions and Optical Efficiencies of the ACPPVC-50 and ACPPVC-60

Rays incident on a solar concentrator from a range of directions are reflected by an imperfect reflector surface leading to further angular dispersion. For a real reflector with a design slope error δ, the reflected rays reach the reflector with an angle 2δ away from the original direction. Optical errors combined with the real radiation source yield an effective radiation source (Winston and Welford, 1982). The effective source $B_{eff}(\theta)$ is the angular distribution that describes how much radiation is incident from the direction θ on the aperture of a perfect reflector. The radiation intercepted by the receiver is defined by the angular acceptance functions f(θ) as the fraction of a uniform beam of parallel rays incident on the aperture at an angle θ from the symmetry axis that would reach the receiver if the optics were perfect (Rabl, 1985). Therefore the intensity of radiation on the aperture from the direction θ reaching the receiver becomes $B_{eff}(\theta)f(\theta)$. The optical efficiency of a system is defined as the fraction of solar radiation incident on the aperture which reaches and is absorbed by the absorber i.e.

$$\eta_0 = \frac{\dot{q}_{abs}}{I} \tag{2.7.1.1}$$

For the asymmetric compound parabolic photovoltaic concentrator most rays have a single reflection before intersecting the photovoltaic absorber. By considering multiple reflections on the reflector, the transmittance reflectance product becomes (Rabl, 1985);

$$\left.\begin{aligned}(\tau\alpha) &= \tau\alpha \sum_{n=0}^{\infty} \left[(1-\alpha)\rho_d\right]^n \\ &= \frac{\tau\alpha}{1-(1-\alpha)\rho_d}\end{aligned}\right\} \tag{2.7.1.2}$$

where α is the absorptance of the photovoltaic material, τ is the transmittance of the glass aperture and ρ is the reflectance of the reflector. Equations (2.2.1.5) and (2.2.1.10) were taken into account to calculate optical efficiencies and the parameters employed in the optical analysis given in table 2.7.1.1.

Angular acceptance was determined for full and truncated versions of ACPPVC-50 and ACPPVC-60. The angular acceptance function and optical efficiency of the untruncated ACPPVC-50 are shown in figure 2.7.1.1. All rays reached the PV absorber for solar incidence angles of 53° to 89°. The highest predicted optical efficiency for this PV concentrator is 85.25%. Since the lower reflector has an half-acceptance angle of 0° (as shown in the ray trace diagram in figure 2.6.2.1 (a)), no rays reach the PV above an incidence angle of 90°. At this solar incidence angle all rays are incident on the upper reflector and are reflected back and exit the aperture without any absorption at the PV. Since the reflectors are not identical, it can be seen from figure 2.7.1.1 that the angular acceptance functions are not symmetric. For lower solar incidence angles i.e. below 10° no rays reach the PV absorber.

Reflectance of mirror reflector (ρ)	0.98
Absorptance of reflector (α)	0.02
Refractive index of glass (n_r)	1.523
Refractive index of air (n_i)	1
Glass extinction coefficient (m^{-1})	4
Absorptance of PV cells	1

Table 2.7.1.1 Optical properties employed in the present analysis.

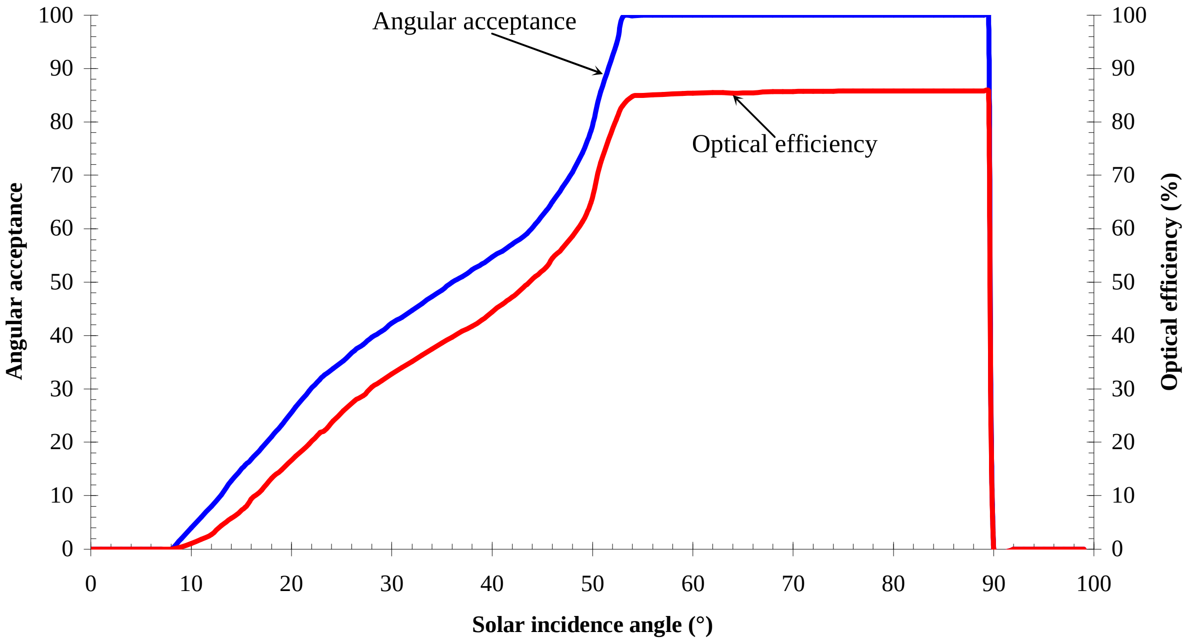

Figure 2.7.1.1 Angular acceptance and optical efficiency for an untruncated ACPPVC-50.

The angular acceptance and optical efficiency for the untruncated ACPPVC-60 is shown in figure 2.7.1.2. Due to the different reflector geometries the angular acceptance functions are not the same for both concentrators. In a similar way to that observed for the ACPPVC-50, since the lower reflector has an acceptance-half angle of 0° (as shown in ray trace diagram, figure 2.6.2.1 (b)), no rays are absorbed when rays are incident above the 90° solar incidence angle. The maximum optical efficiency of 85.25% is achieved for solar incidence angles in the range between 57° to 90°. 100% collection of all rays entering can be achieved between 38° to 90° solar incidence angles.

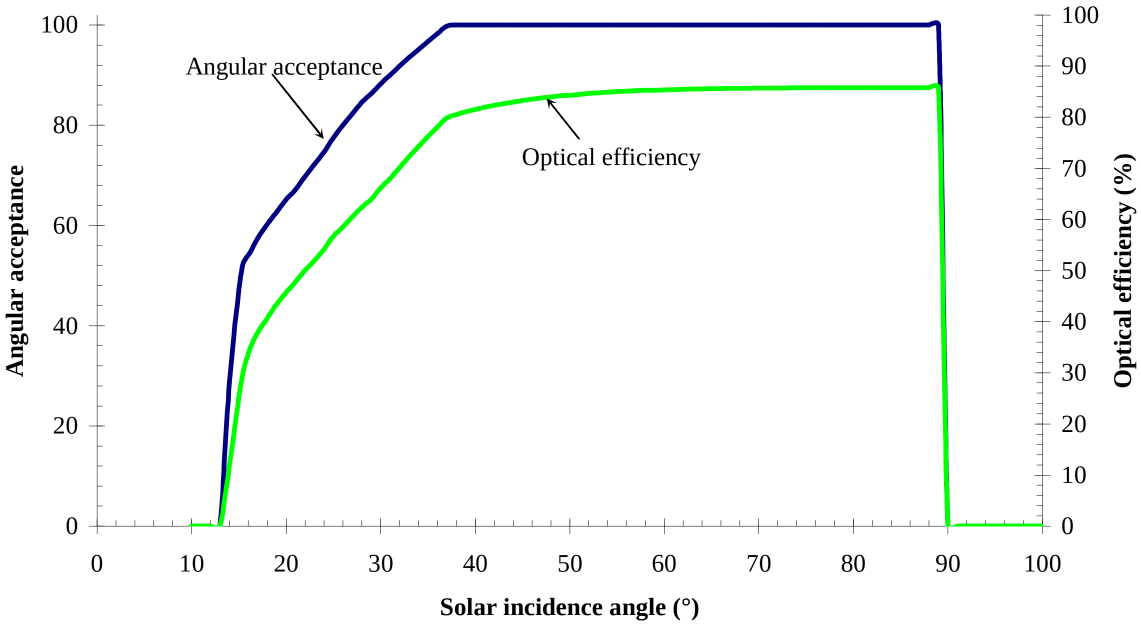

Figure 2.7.1.2 Variation of angular acceptance and optical efficiency for an untruncated ACPPVC-60.

Figure 2.7.1.3 illustrates the variation of angular acceptance and optical efficiency with solar incidence angle when the ACPPVC-50 is truncated by 54%. The angular acceptance functions are increased compared to the untruncated system as shown in figure 2.7.1.1. However the highest optical efficiency for both the untruncated and truncated systems remains 85.25%. It can be seen from figure 2.7.1.3 that all rays incident at the aperture cover reach the photovoltaic surface at the absorber above the solar incidence angle of 43° and below 90°. Therefore 54% truncation of an ACPPVC-50 increases the angular acceptance range by 22%. It is clear from figure 2.7.1.3 that no rays can reach the absorber below a solar incidence angle of 15° or above an incidence angle of 130°.

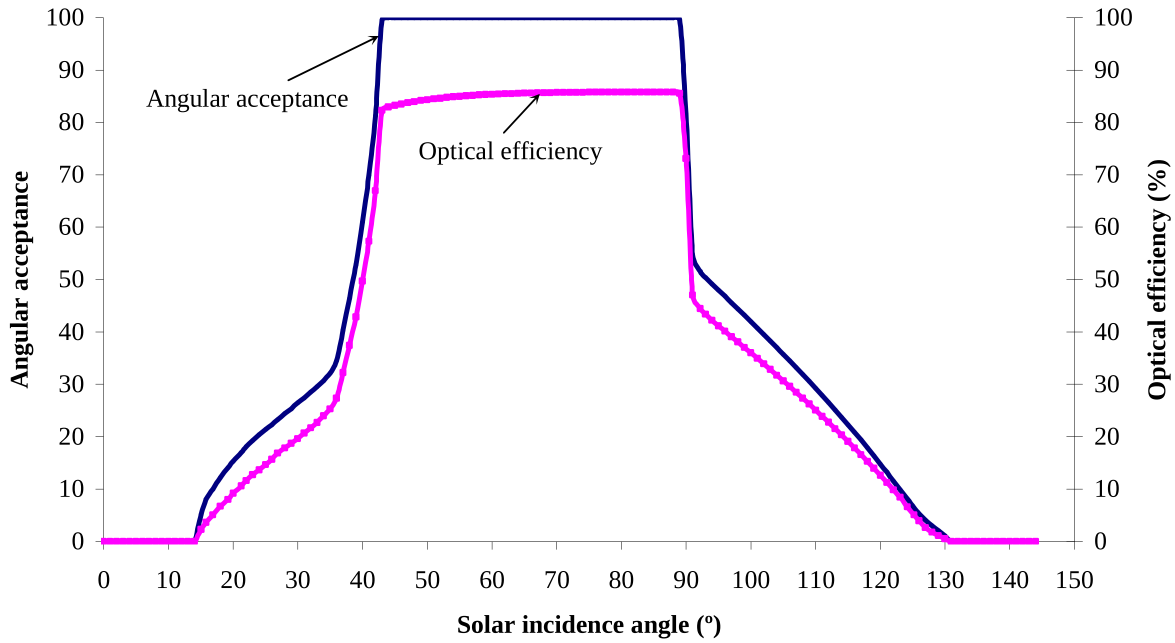

Figure 2.7.1.3 Variation of angular acceptance and optical efficiency for a truncated ACPPVC-50.

Photovoltaic concentrators using different numbers of planar elements to comprise the reflector profile were investigated. The angular acceptance and optical efficiency of the untruncated version of an ACPPVC-50 using 5-planar elements for the reflector profile is presented in figure 2.7.1.4. Although the highest optical efficiency achieved was 85.25% for this system, the angular acceptance range decreases compared to that for a curved reflector. Similar to the untruncated ACPPVC-50 and ACPPVC-60, no rays can reach the absorber when the solar incidence angle is above 90°. This is because, the effective acceptance-half angle of the lower parabola is 0°.

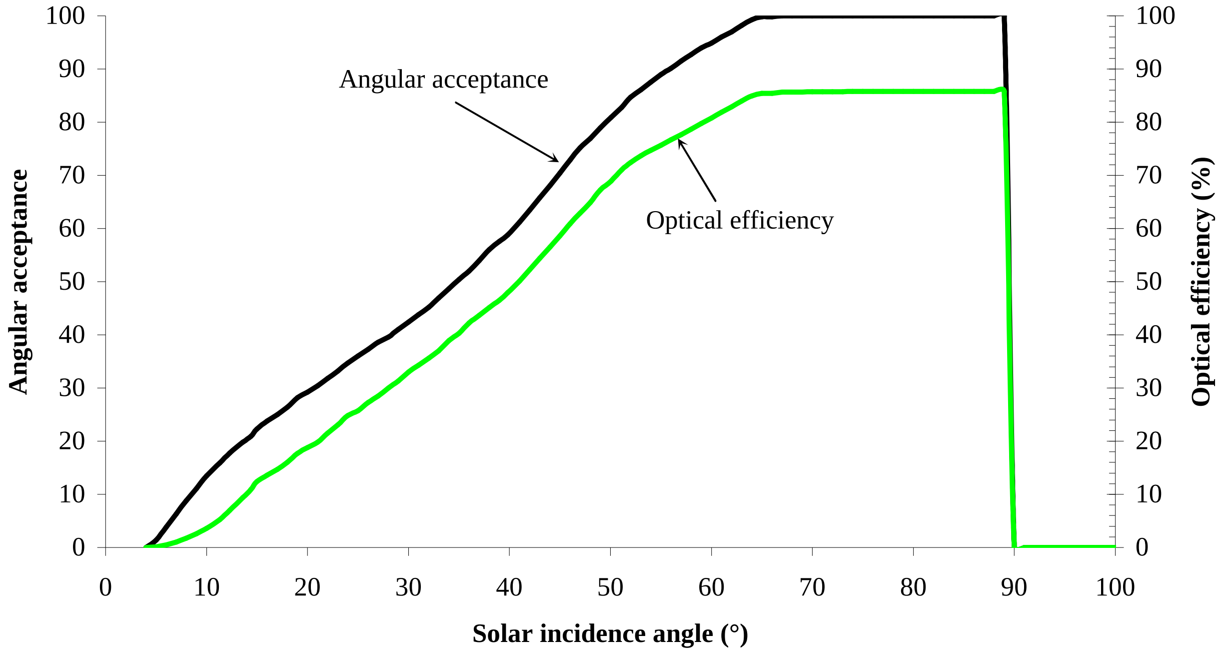

Figure 2.7.1.4 Variation of angular acceptance and optical efficiency of an untruncated ACPPVC-50 with reflectors comprised of 5-planar elements.

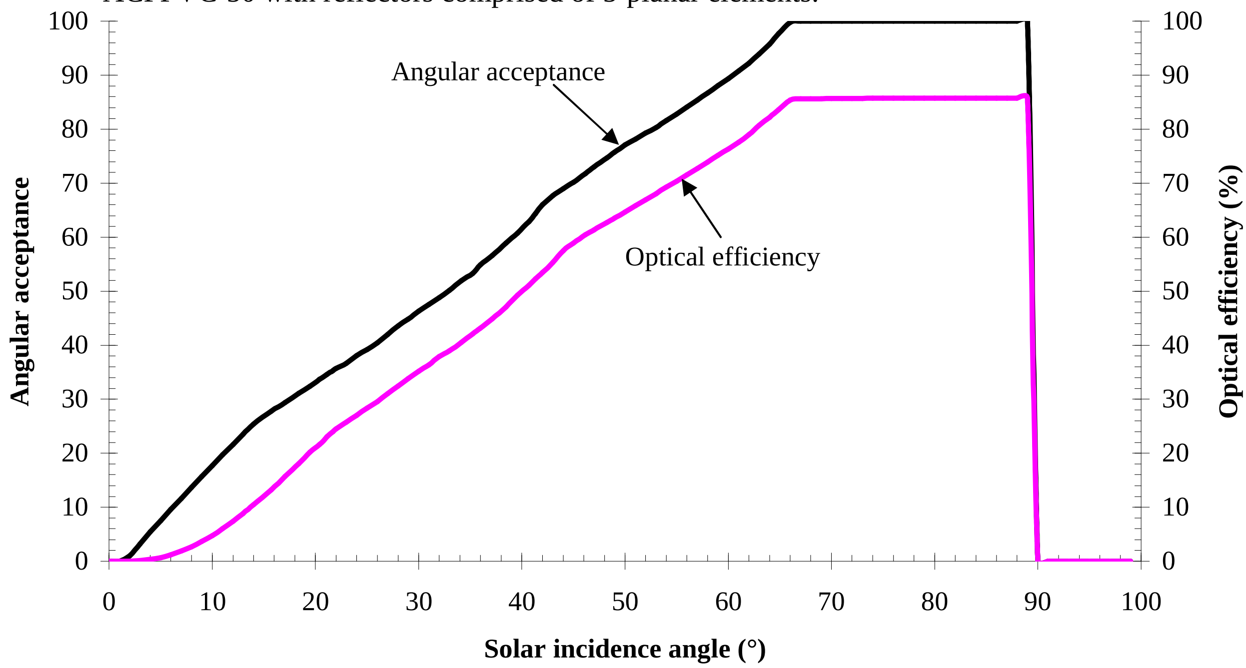

Figure 2.7.1.5 Variation of angular acceptance and optical efficiency of an untruncated ACPPVC-50 with reflectors comprised of 3-planar elements.

A further decrease in the number of planar elements used to make the reflector profile to 3 leads to a further reduction in the angular acceptance range. However the angular acceptance and optical efficiency variation can be seen to be similar for the 3-planar element reflector as shown in figure 2.7.1.5. The same numbers of planar elements (80) were considered to make the upper parabola, as can be seen from ray trace diagram shown in figure 2.6.4.1.

Simulations for the truncated systems using different numbers of planar elements to make the reflector profile were undertaken. The variation of angular acceptance and optical efficiency for reflectors comprised of 5-planar elements are shown figure 2.7.1.6. The range of acceptance angles to maintain the highest optical efficiency decreased for lower numbers of planar reflector elements compared to higher numbers of planar reflector elements.

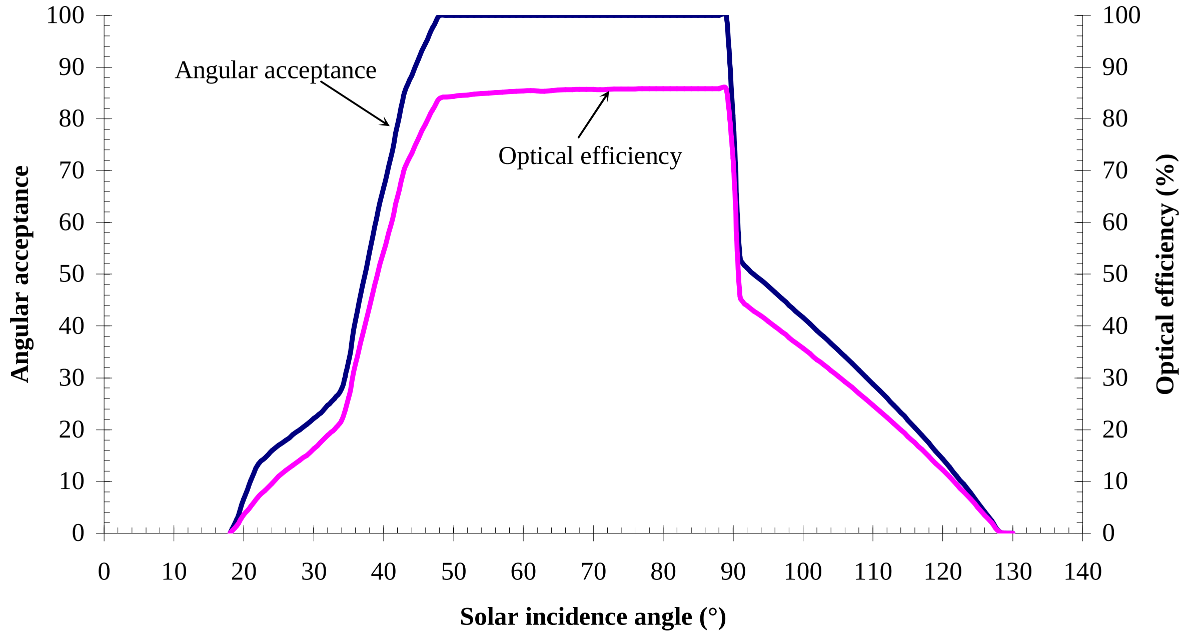

Figure 2.7.1.6 Variation of angular acceptance and optical efficiency of a truncated ACPPVC-50 with reflectors comprised of 5-planar elements.

The variation of angular acceptance and optical efficiency of a truncated version of the ACPPVC-50 with the lower reflector comprised of 3 planar elements is shown in figure 2.7.1.7. When the numbers of planar elements decrease from five to three the angular acceptance range decreases by 13%, however the highest predicted optical efficiency remains the same for both concentrators as shown in figure 2.7.1.8.

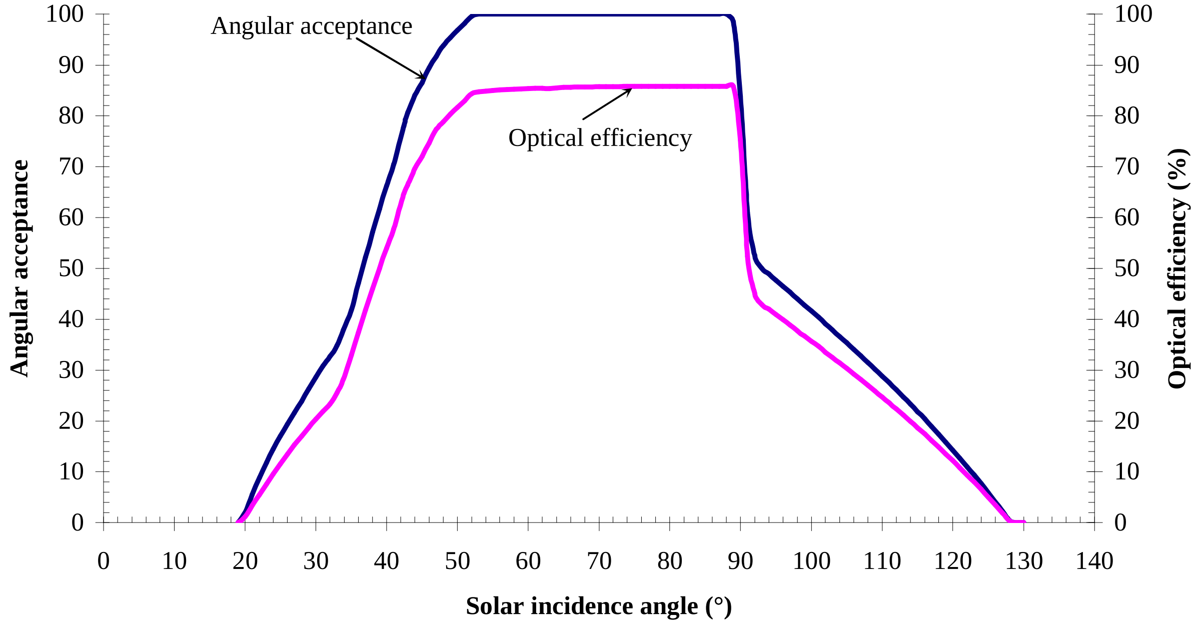

Figure 2.7.1.7 Variation of angular acceptance and optical efficiency of a truncated ACPPVC-50 with reflectors comprised of 3-planar elements.

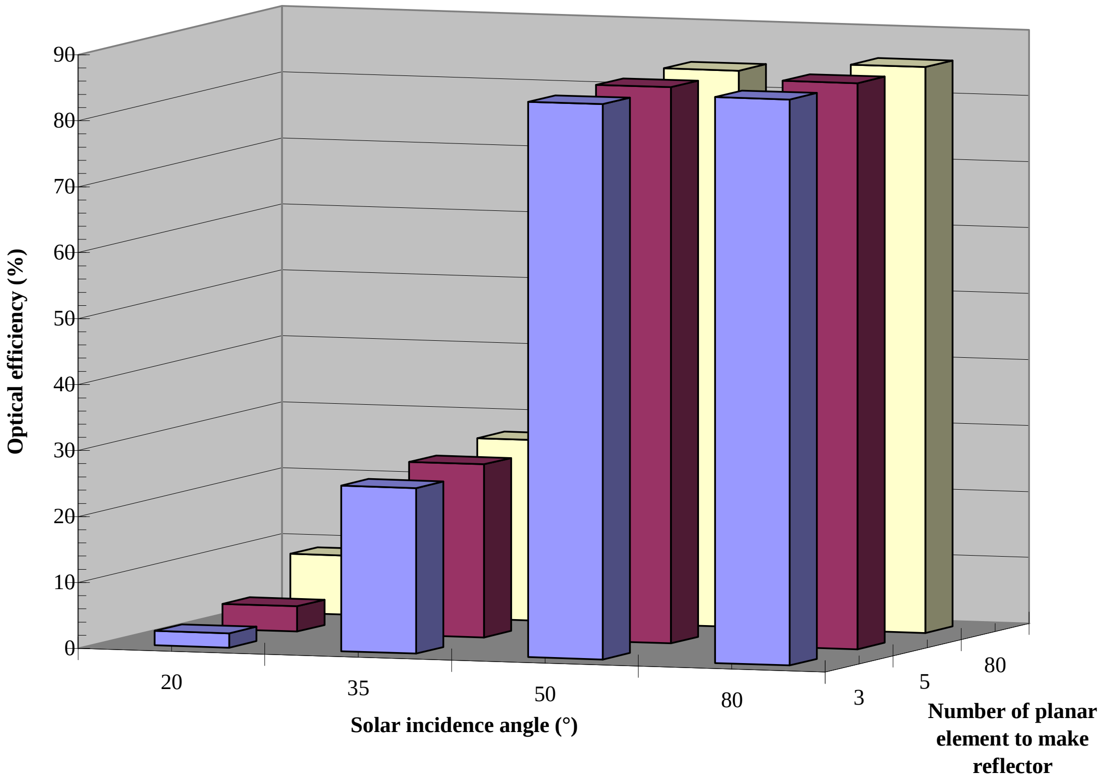

Figure 2.7.1.8 Variation of optical efficiency with solar incidence angle and number of planar elements used to comprise the reflector profiles.

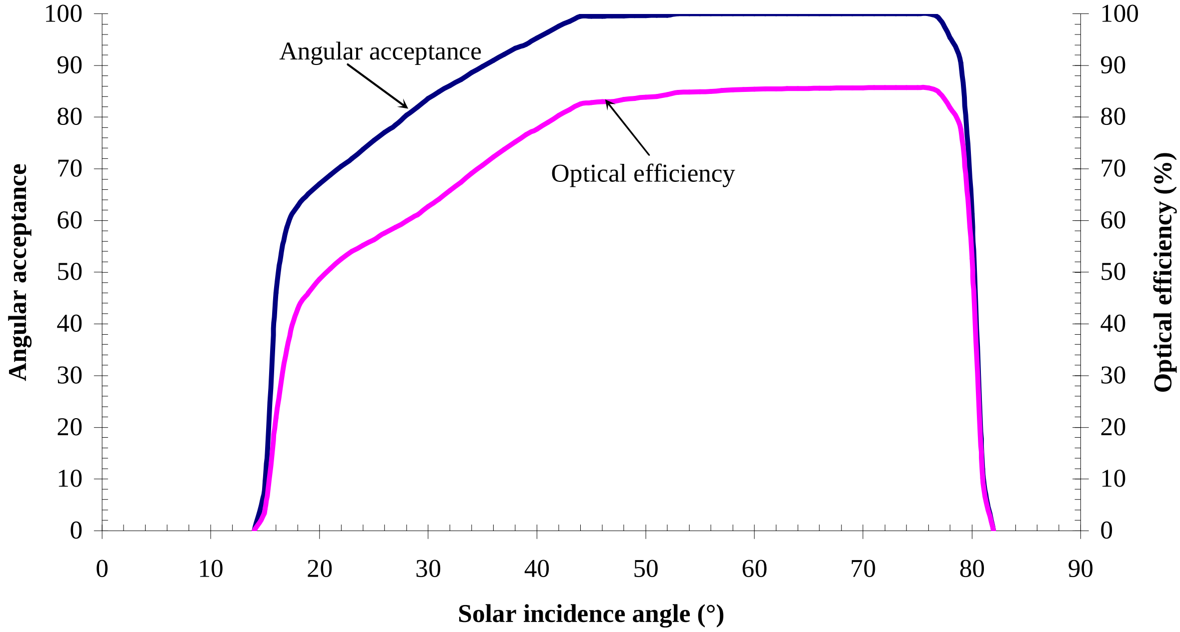

Figure 2.7.1.9 Variation of angular acceptance and optical efficiency for ten degree inclined untruncated ACPPVC-50 for different solar incidence angle.

The angular acceptance and optical efficiency of a 10º inclined ACPPVC-50 is shown in figure 2.7.1.9. As can be seen from the ray trace diagram (i.e. figure 2.6.5.1), increasing the inclination angle increases the number of reflections on the lower reflector before rays reach the PV absorber. The number of reflections on the upper reflector increases in the similar angular range but maintained the highest optical efficiency of 85.25%. It can be seen from figure 2.7.1.9 that no rays can reach the absorber below an incidence angle of 10º or above an incidence angle of 82º.

The variation of angular acceptance and optical efficiency of a truncated ACPPVC-50 when inclined at ten degrees is shown in figure 2.7.1.10. As expected the angular acceptance range increases for the truncated version of the ACPPVC-50 inclined at 10°. No rays can reach the absorber below an incidence angle of 20º or above an incidence angle of 118º. It can be seen from figure 2.7.1.9 that no rays can be absorbed by the PV absorber above a solar incidence angle of 82º for the untruncated ACPPVC-50 but some rays can reach the absorber for truncated inclined system.

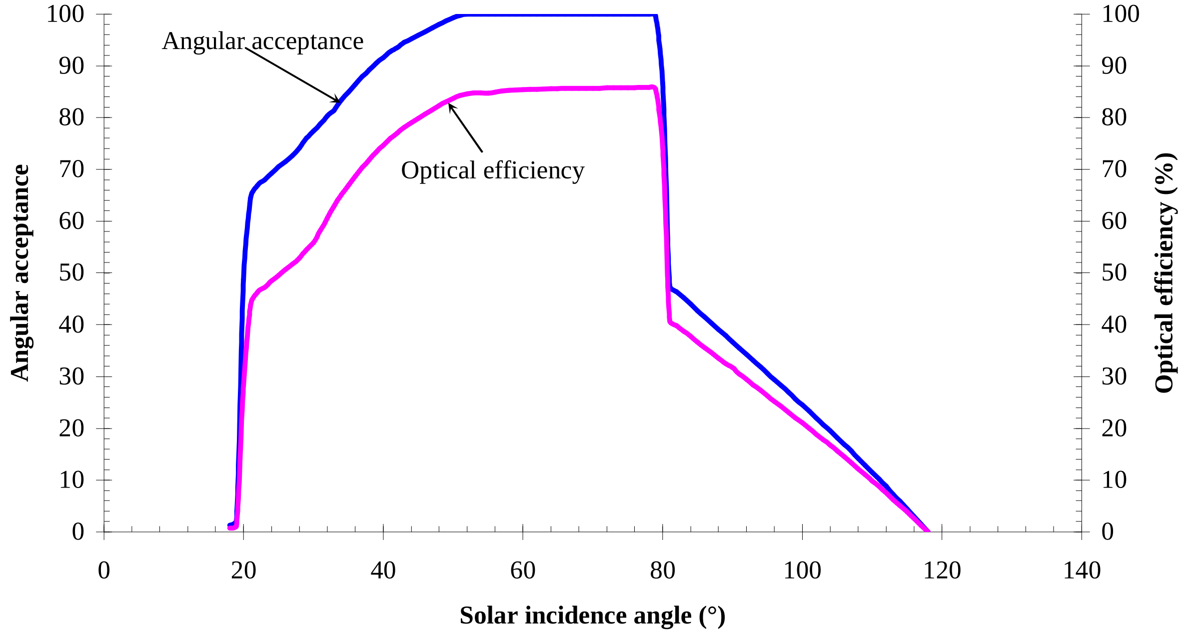

Figure 2.7.1.10 Variation of angular acceptance and optical efficiency of a ten degree inclined truncated ACPPVC-50.

2.8 Energy Distribution Across the Different Components of an ACPPVC-50

The energy absorbed at the different components of the ACPPVC-50 system are calculated during the ray trace analysis using the equations detailed in section 2.2.

2.8.1 Determination of Direct Solar Radiation Distributions onto System Components

Radiation can be incident at any angles between 0º to 180º (i.e. -90º to +90º) on to the aperture plane. 100,000 equal spaced rays incident on the aperture in each with an equal amount of energy were traced and the energy absorbed at the different components calculated.

2.8.1.1 Reflection Losses and Absorbed Energy Distribution Across the Glass Aperture Cover

The energy distribution at the aperture cover glass of a truncated ACPPVC-50 for solar incidence angles of 42°, 60° and 89.5° are shown in figure 2.8.1.1.1. The incident solar radiation flux was considered to be 1000 Wm^{-2}. It can be seen from figure 2.8.1.1.1 that, as expected, the energy absorbed at higher incidence angles increased as indicated in the ray trace diagrams. The absorbed energy flux is increased by 32 Wm^{-2} when the solar incidence angle is changed from 42º to 89.5º. As expected from the ray trace diagram, figure 2.6.3.1, a high energy flux can be seen towards the lower reflector, this is because at 42º solar incidence angle, few rays are reflected back and exit from the aperture. As the incidence angle increases, the overall energy flux becomes more uniform. When the solar incidence angle is above 42º or less than 90º, the collection efficiency became 100% as revealed by the ray trace analysis and thus energy flux for these incidence angles are more uniform. However a small peak can be seen for each incidence angle, this is because near the edge of the aperture some of the rays miss the absorber and exit from the aperture. As the solar incidence angle is increased to 89.5º, higher absorption of energy occurs near to the upper reflector as expected from the ray trace diagram. For a 90º solar incidence angle, some of the solar rays are re-reflected back from the upper reflector and exit the absorber.

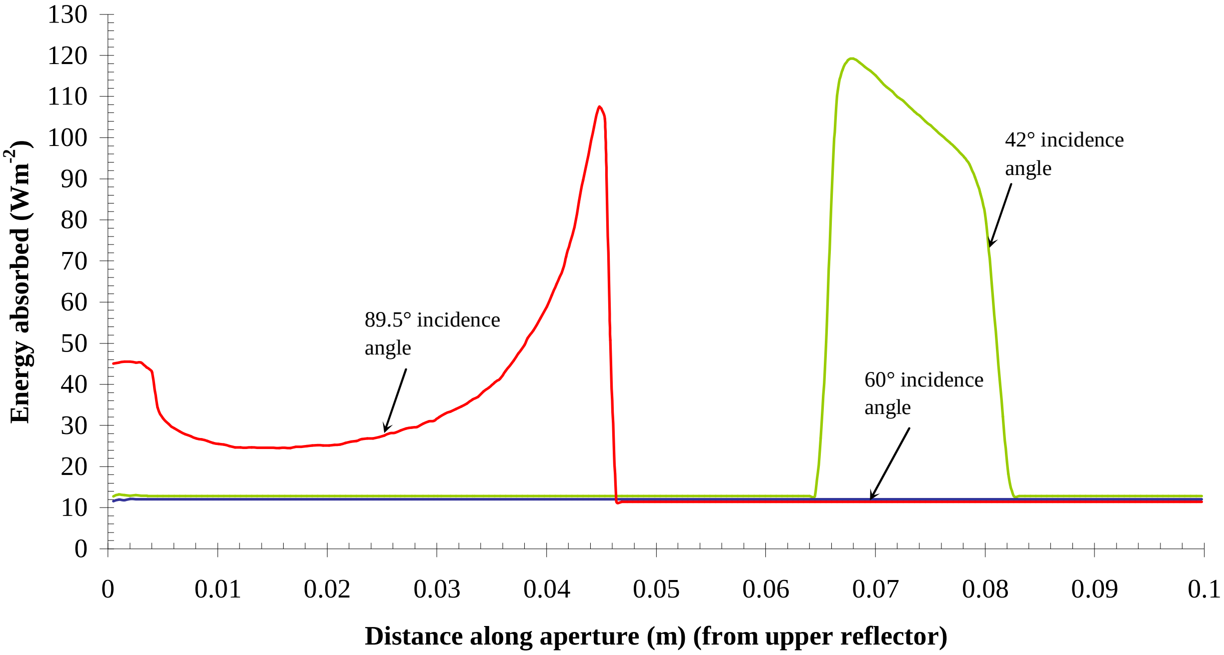

Figure 2.8.1.1.1 Energy distribution across the aperture of a truncated ACPPVC-50 for solar incidence angles of 42°, 60° and 89.5° to the vertical. The incident solar radiation intensity was 1000 Wm^{-2}.

2.8.1.2 Absorbed Energy Distribution Across the Reflectors

The variation of energy absorbed on the lower reflector by a truncated ACPPVC-50 for solar incidence angles of 42°, 60°, 75° and 89.5° are shown in figure 2.8.1.2.1. Figure 2.8.1.2.2 shows the energy absorbed by the upper reflector for solar incidence angles of 60°, 75° and 89.5°. The incident energy was considered to be 1000 Wm^{-2}. As expected from the ray trace diagrams the upper reflector absorbs a higher energy flux compared to the lower reflectors at higher incidence angles such as 75° and 89.5° (figure 2.8.1.2.1 and figure 2.8.1.2.2). This is due to the number of reflections at the upper reflector being higher before intersection with the PV absorber when compared to the number of reflections at the lower reflectors before intersection with the PV absorber.

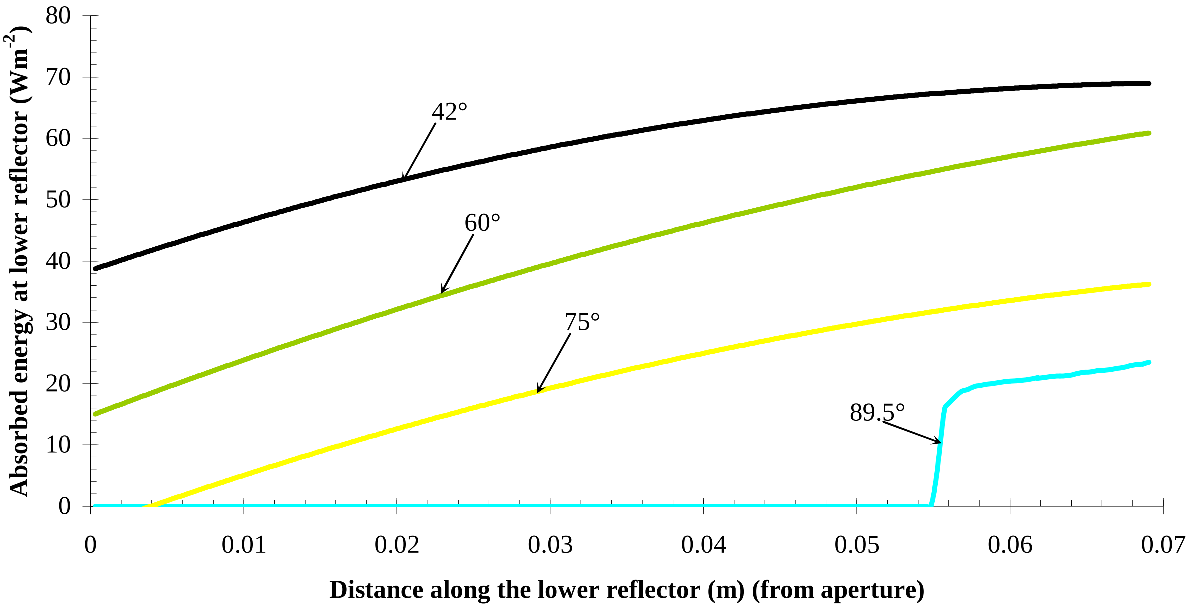

Figure 2.8.1.2.1 Energy absorbed along the lower reflector of a truncated ACPPVC-50 for solar incidence angles of 42°, 60°, 75° and 89.5°. The incident solar radiation intensity was 1000 Wm^{-2}.

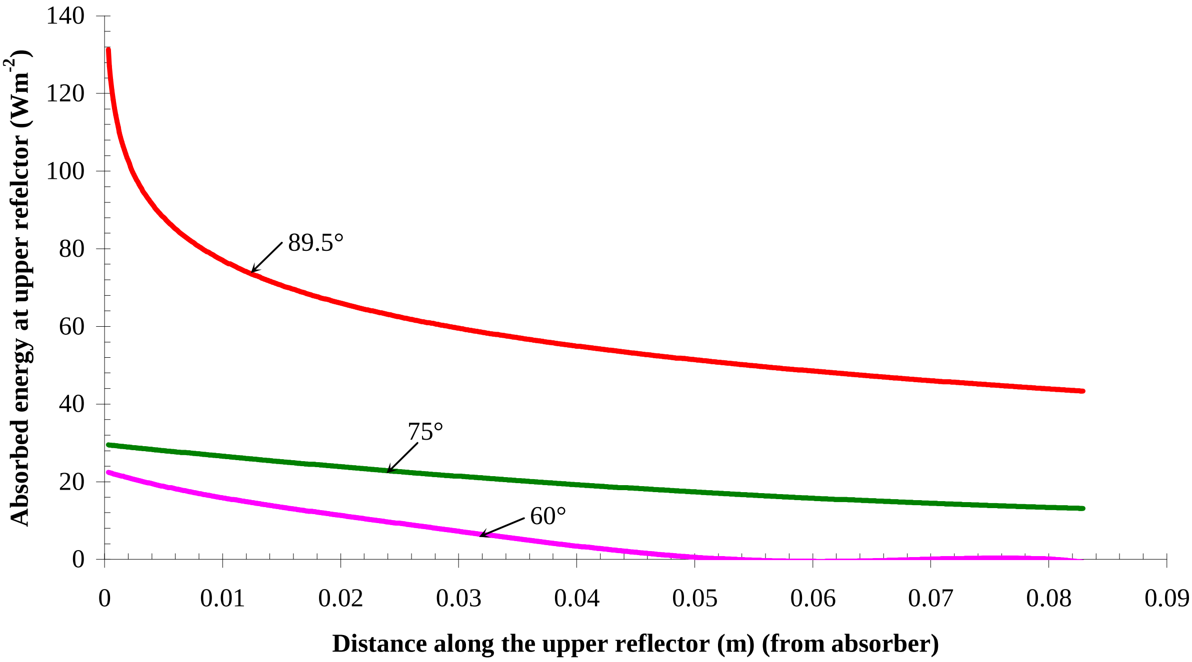

Figure 2.8.1.2.2 Energy absorbed along the upper reflector of a truncated ACPPVC-50 for solar incidence angles of 60°, 75° and 89.5°. The incident solar radiation intensity was 1000 Wm^{-2}.

For a truncated ACPPVC-50 when inclined at 10º to a vertical façade the absorbed energy flux at the individual reflectors increases for a solar incidence angle of 60º. The energy distributions along both reflectors of a truncated ACPPVC-50 inclined at 10° and 0° to the vertical are shown in figure 2.8.1.2.3. The incident solar radiation was considered to be 1000 Wm^{-2} with an incidence angle of 60º to the vertical. For both reflectors, the energy intensity increases near the absorber, this is due to the increasing number of reflections at the reflector before reaching at the absorber.

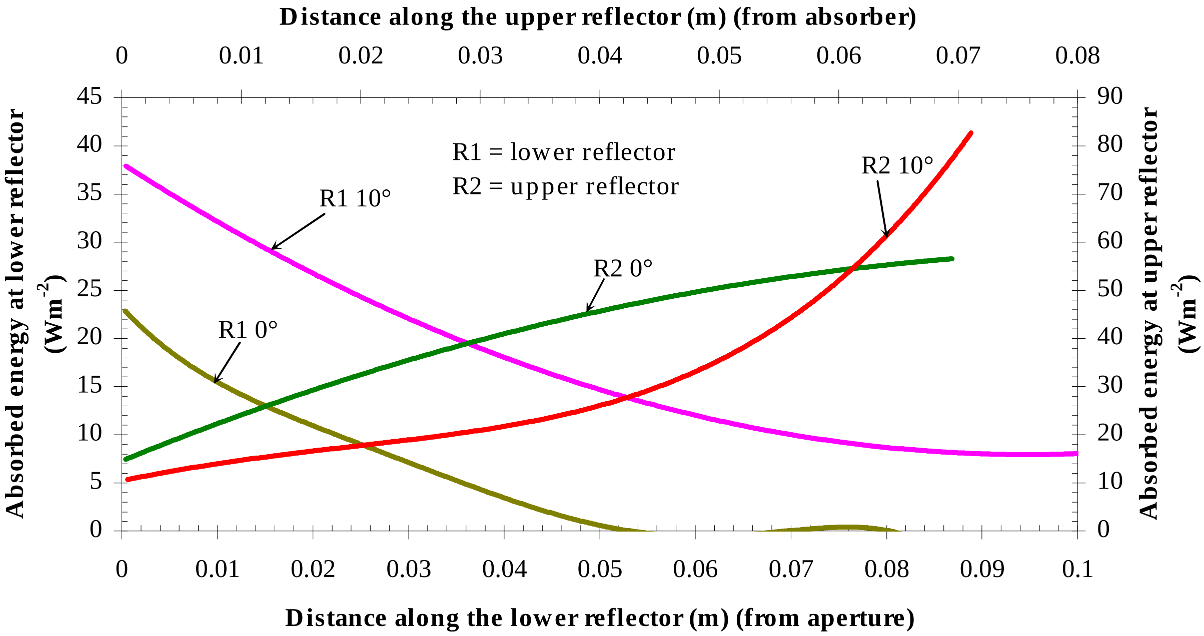

Figure 2.8.1.2.3 Predicted energy absorbed at the reflectors of a truncated ACPPVC-50 inclined at 10° and 0° to the vertical. The incident solar radiation intensity was 1000 Wm^{-2} incident at an angle of 60° to the vertical.

2.8.1.3 **Absorbed Energy Distribution at the PV Absorber**

Figure 2.8.1.3.1 illustrates the energy distribution at the photovoltaic absorber of a truncated ACPPVC-50 for solar incidence angles of 42°, 60°, 75° and 89.5° to the vertical. For all predictions the solar radiation intensity assumed was 1000 Wm^{-2}. As it can be seen in figure 2.8.1.3.1, peaks occur near to either end of the PV absorber. It can also be seen that as the solar incidence angle increases the major peaks shift towards the upper side of the absorber i.e. away from lower reflector. This trend can be identified clearly in the corresponding ray trace diagrams shown in figure 2.6.3.1. The secondary peak occurs because of the reflections from the upper reflector. However, because of exiting rays at lower incidence angles (i.e. below 42º) and when the incidence angle is above 90º the energy absorbed at the PV surface reduces compared to that in the angular acceptance range of 43º to 90º.

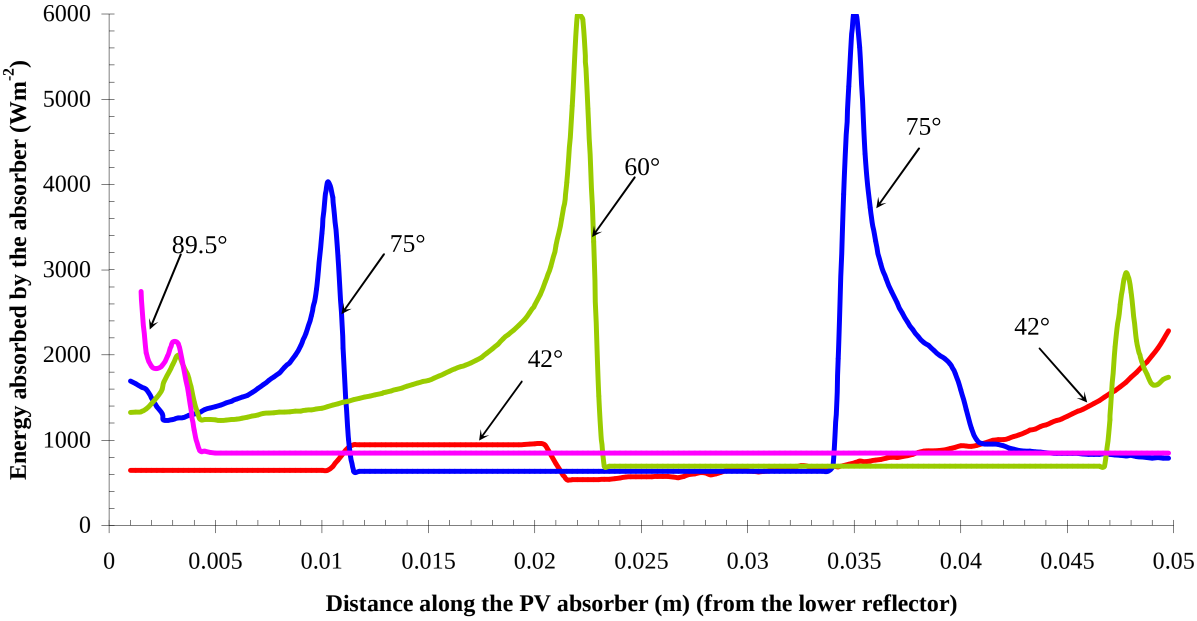

Figure 2.8.1.3.1 Energy distribution across the photovoltaic absorber of a truncated ACPPVC-50 for solar incidence angles of 42°, 60°, 75° and 89.5° to the vertical. The incident solar radiation intensity was 1000 Wm^{-2}.

The reflector can be approximated by different numbers of planar reflector elements. The energy distributions at the PV absorber when the lower reflector is made of 3 and 5-planar elements are shown in figure 2.8.1.3.2. Due to the discretization used to make the lower reflector of different planar elements, the energy absorbed by the PV surface is not uniform. The total amount of energy absorbed at the PV absorber is different when the reflector is made up of higher numbers of planar elements.

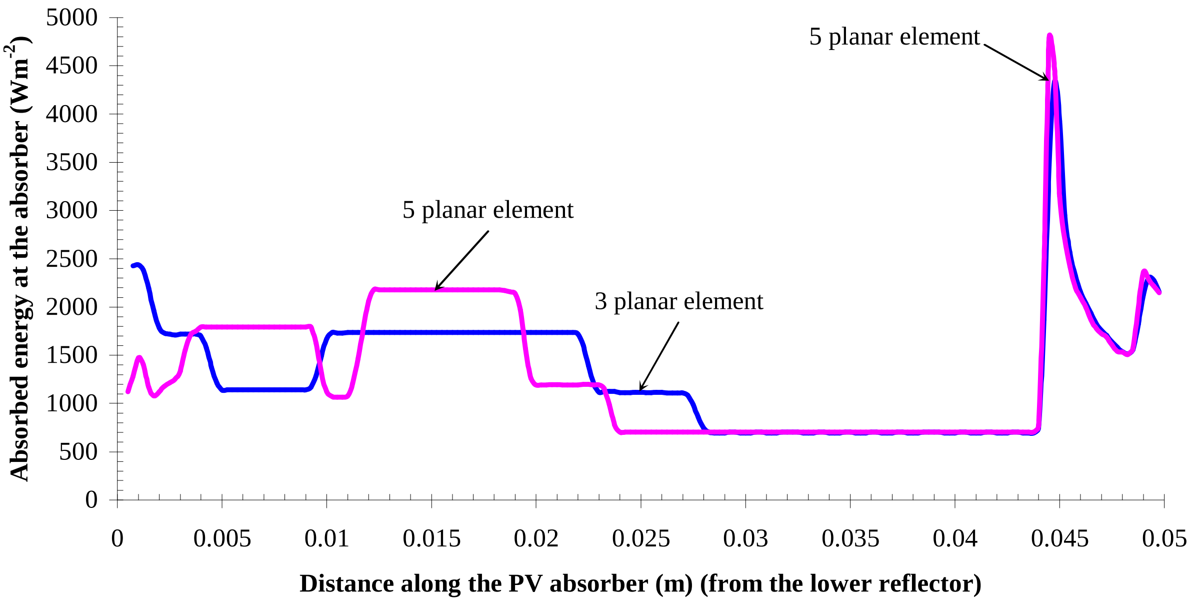

Figure 2.8.1.3.2 Absorbed energy at the PV absorber of a truncated ACPPVC-50 with reflectors comprised of three and five planar elements. The incident solar radiation intensity was 1000 Wm^{-2} incident at an angle of 60º to the vertical.

Figure 2.8.1.3.3 shows that the energy distribution at the absorber when the untruncated ACPPVC-50 is inclined at 10º to the vertical and with no inclination for the untruncated version of an ACPPVC-50 and the energy absorbed at the absorber for the truncated version is shown in figure 2.8.1.3.4. The incident solar radiation intensity was 1000 Wm^{-2} and the solar incidence angle was 60º to the vertical. It can be observed from figure 2.8.1.3.3 that in addition to two major peaks, a third minor peak can be seen near to the lower reflector for the untruncated system. This is because the number of reflections increases at the lower reflector as the system is inclined at a 10º inclination angle. The amount of energy absorbed by the truncated ACPPVC-50 is increased by 10% compared to the untruncated counterpart due to the angular acceptance increasing for the truncated system. In all configurations the two major peaks can be seen to coincide with the ray trace diagrams.

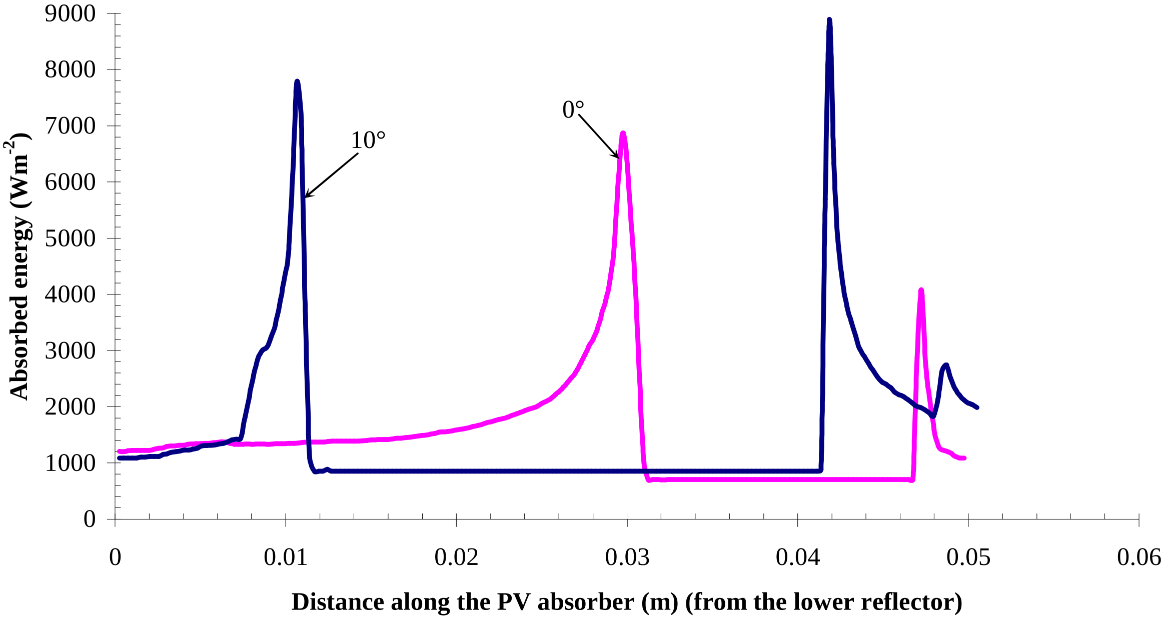

Figure 2.8.1.3.3 Absorbed energy at the absorber of an untruncated ACPPVC-50 inclined at 10° and 0° to the vertical. The incident solar radiation intensity was 1000 Wm^{-2} incident at an angle of 65º to the vertical.

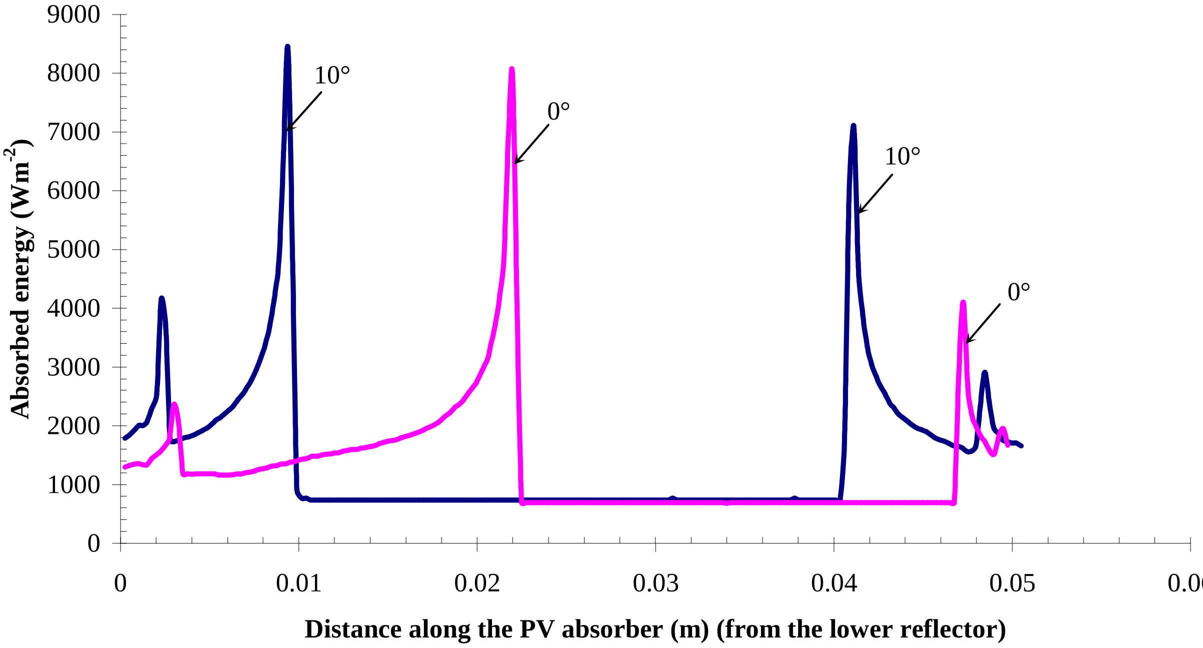

Figure 2.8.1.3.4 Absorbed energy at the PV absorber of a truncated ACPPVC-50 inclined at 10° and 0° to the vertical. The incident solar radiation intensity was 1000 Wm^{-2} incident at an angle of 65º to the vertical.

2.8.2 Distribution of Diffuse Solar Radiation to Different Components of an ACPPVC-50 System

To determine the effect of the diffuse insolation on the energy distributions at the different components of the developed line axis solar photovoltaic systems, three different angular skyward diffuse distributions were considered as described in equation (2.3.1) (Prapas et al., 1987a). For each solar incidence angle between 0º to 180º (i.e. -90º to +90º) at 2º intervals, 100,000 rays incident at the aperture cover were traced. The calculated energy flux at each component and the total energy flux for each segment of the system were determined from the sum of the energy fluxes for each angle of incident radiation.

No solar rays can be absorbed by the photovoltaic absorber for the systems modelled when the solar incidence angle is below 12° or above 130°. Therefore the total energy absorbed at the absorber from the diffuse solar radiation can be calculated from

$$E_{tot} = I_d \int_{12^0}^{130^0} I(\theta) d\theta \tag{2.8.1}$$

It can be seen from figure 2.3.1 (page 49) that the energy contained between the angles of 12° to 130° is higher for the cosine and hybrid Gaussian distributions compared to the isotropic distribution.

2.8.2.1 Energy Distribution of Diffuse Solar Radiation Absorbed at the Aperture Cover of the ACPPVC-50 System

The distribution of energy flux at the aperture cover of the truncated ACPPVC-50 for the three different skyward angular diffuse distributions modelled is shown in figure 2.8.2.1.1. The incident solar radiation flux was considered to be 100 Wm^{-2}. The highest energy absorbed can be seen to be from the isotropic distribution although the trend for the three distributions is the same. The concentrator absorbs all rays incident between 42° to 89° as revealed from the angular acceptance function calculations. Figure 2.7.1.3 reveals that no rays can be absorbed by the absorber below a solar incidence angle of 14° or above 130°. The peak energy intensity of 9.4 Wm^{-2} occurs for the cosine distributions when the incident diffuse solar radiation was 100 Wm^{-2}.

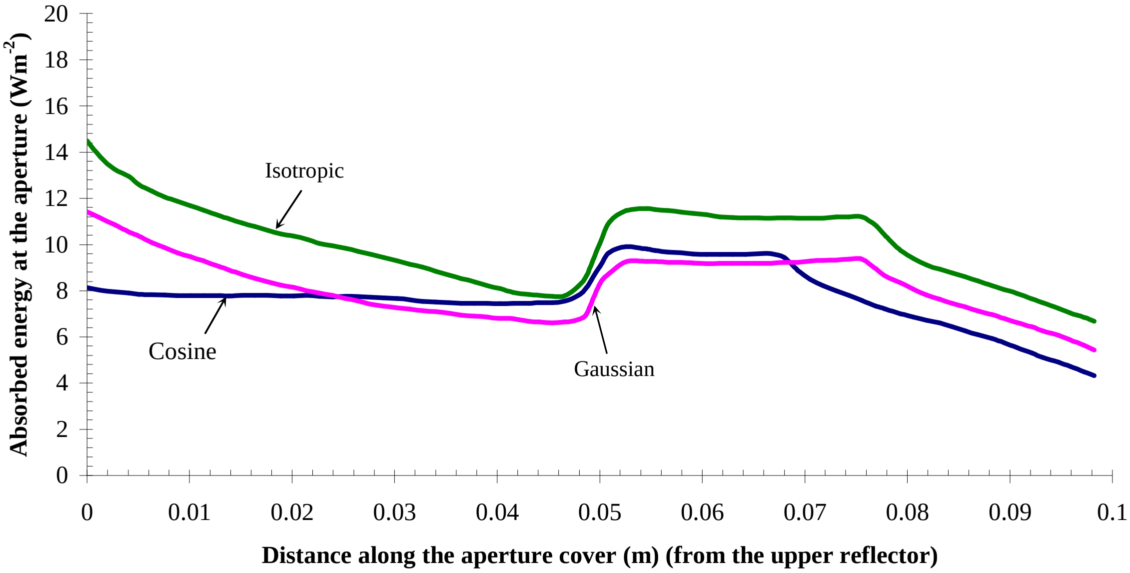

Figure 2.8.2.1.1 Energy distribution of the truncated ACPPVC-50 along the aperture cover for diffuse solar radiation. The incident diffuse solar radiation intensity was 100 Wm^{-2}.

2.8.2.2 **Energy Distribution of Diffuse Solar Radiation Absorbed at the Reflectors of an ACPPVC-50 System**

The predicted energy distributions for the lower and upper reflectors of an ACPPVC-50 for the three different skyward angular diffuse distributions are illustrated in figure 2.8.2.2.1 and figure 2.8.2.2.2 respectively. As illustrated in figure 2.8.2.2.1, the energy absorbed for an isotropic distribution is higher than that compared to cosine and hybrid Gaussian angular distributions for both reflectors. For these predictions 80 reflector element segments were used for each individual component and 100,000 rays incident at the aperture cover were traced at 2° intervals. The maximum energy absorbed at the lower reflector was 3.6 Wm^{-2} when the incident diffuse radiation was 100 Wm^{-2}.

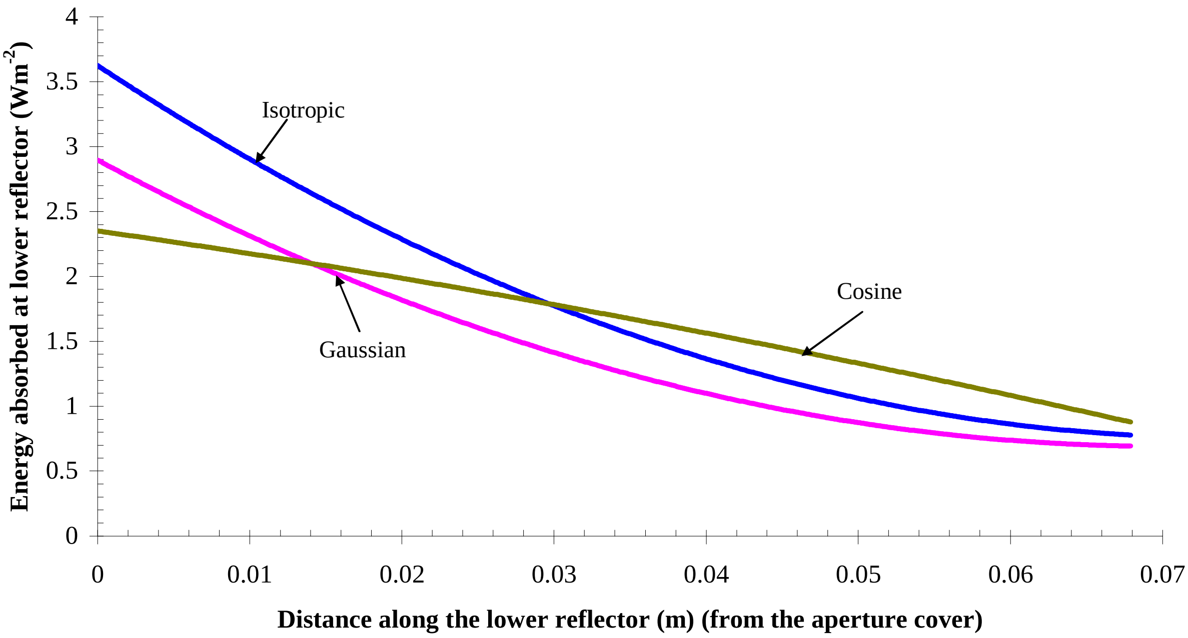

Figure 2.8.2.2.1 Predicted energy absorbed at the lower reflector for three diffuse solar radiation distributions. The incident diffuse solar radiation intensity was 100 Wm^{-2}.

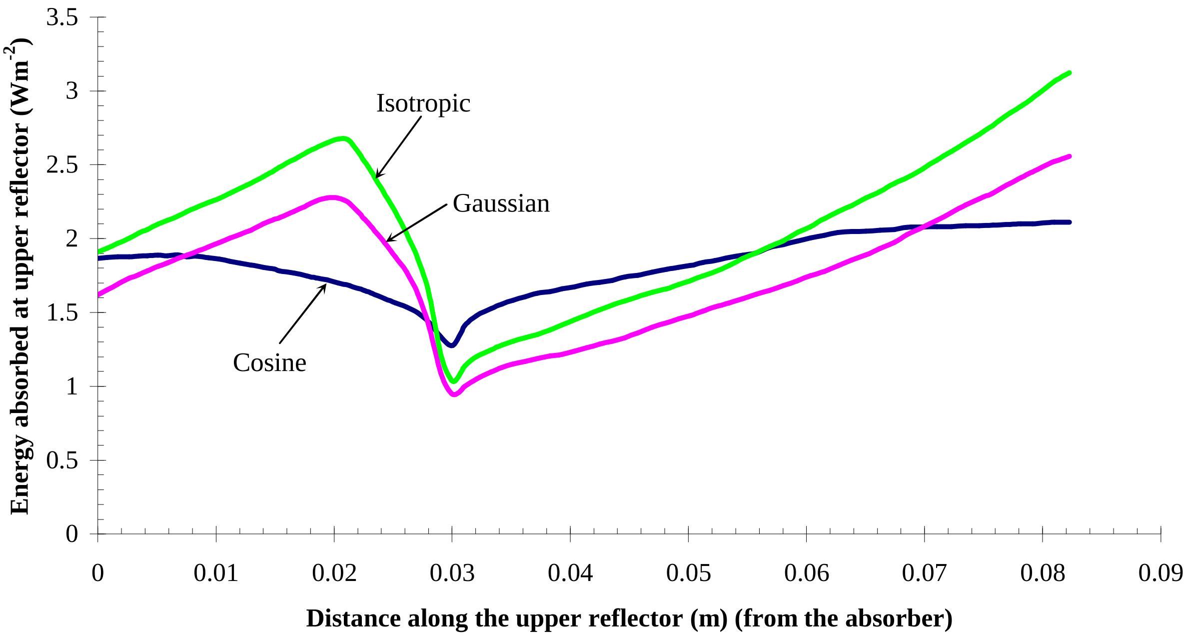

Figure 2.8.2.2.2 Predicted energy absorbed at the upper reflector for three different diffuse solar radiation distributions. The incident diffuse solar radiation intensity was 100 Wm^{-2}.

2.8.2.3 Energy Distribution of Diffuse Solar Radiation Absorbed at the PV Absorber of an ACPPVC-50 System

Figure 2.8.2.3.1 illustrates the diffuse energy distributions of a truncated ACPPVC-50 at the PV absorber for three skyward angular distributions. The incident solar radiation intensity was 100 Wm^{-2}. For each angular distribution, 100,000 rays incident at the aperture were traced at 2° intervals for solar incidence angles from 0° to 180°. For the cosine angular distribution more energy is absorbed over a wide section of the PV absorber, however near to the lower reflector an hybrid Gaussian angular distribution shows higher peak energy levels. The highest energy intensity of 156 Wm^{-2} occurs adjacent to the lower reflector.

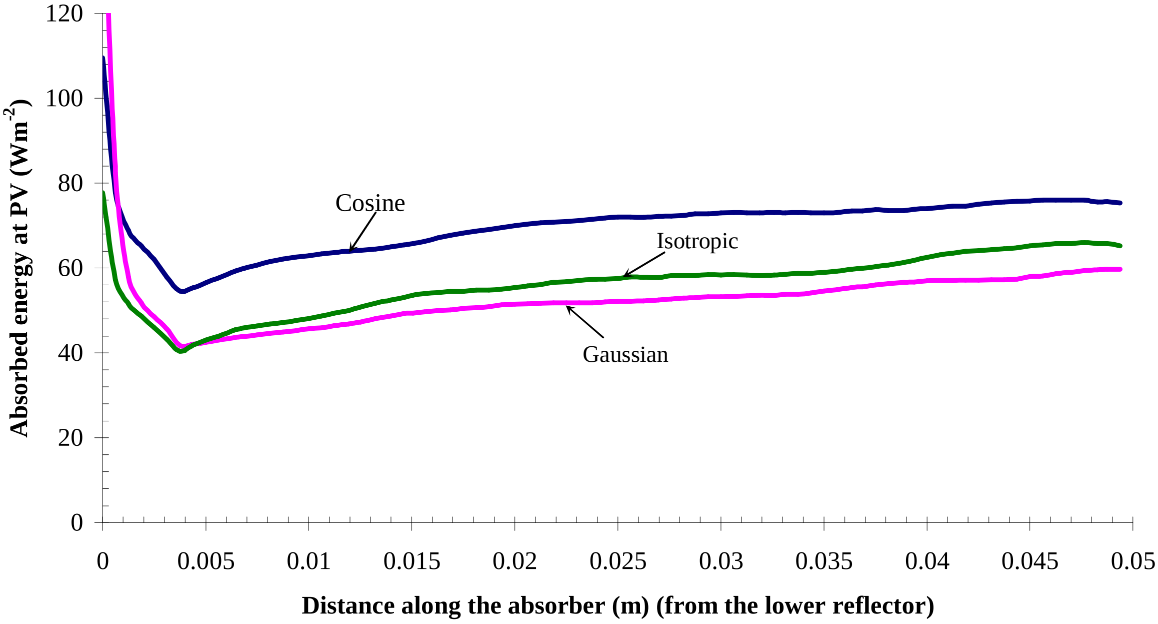

Figure 2.8.2.3.1 Predicted energy absorbed at the photovoltaic absorber for three diffuse solar radiation distributions. The incident diffuse solar radiation intensity was 100 Wm^{-2}.

2.9 Conclusions

Extensive optical analysis of 60° and 50° effective acceptance half-angle asymmetric compound parabolic photovoltaic concentrators showed that both concentrators achieved maximum optical efficiencies of up to 85.25%. Truncating the reflector by 54% increases the angular acceptance range by 22%, maintaining a higher optical efficiency over the collection range for the ACPPVC-50 system. Higher numbers of planar element reflectors increased the angular acceptance range implying a perfect parabolic geometry to be seen. An ACPPVC-50 inclined at 5° and 10° with the vertical increases the angular acceptance range compared to that of an ACPPVC-50 with no inclination.

The energy distribution of direct solar radiation for different components of the system showed that energy absorbed at the aperture for normal incidence to the vertical leads to lowest energy absorbed because of lowest optical path length, however due to rays exiting the collector the absorbed energy is higher than that of inclination angle of 42°. Since both systems are asymmetric, energy distributions are different near to the reflector for normal incidence implies number of rays undergoes by the reflector are different for both reflectors. The energy flux for three skywards diffuse solar radiation showed that cosine angular distribution achieved higher energy peaks for all system components.